Fermilab Proposal No. 694
Spokesman: J. Sandweiss

A PROPOSAL TO STUDY THE PROPERTIES OF HEAVY QUARK PRODUCTION AND DECAY USING A HIGH RESOLUTION STREAMER CHAMBER

D. Brick, H. Rudnicka, A.M. Shapiro and M. Widgoff
Brown University, Providence, R.I. 02912

A.T. Goshaw, P.W. Lucas, W.J. Robertson and W.D. Walker
Duke University, Durham, N.C. 27706

M. Johnson, H. Johnstad and L. Voyvodic
Fermi National Accelerator Laboratory, Batavia, ILL 60510

D. Alyea
Indiana University, Bloomington, IN 47401

E.S. Hafen, P. Haridas, R.I. Hulsizer, I.A. Pless and R.K. Yamamoto
Massachusetts Institute of Technology, Cambridge, MA 02139

C. Bromberg, R.A. Lewis, R. Miller, B.Y. Oh, G.A. Smith and J. Whitmore
Michigan State University, E. Lansing, MI 48824

H.O. Cohn
Oak Ridge National Laboratory, Oak Ridge, TN 37830

P.F. Jacques, M. Kalelkar, R.J. Plano, P. Stamer and A. Vogel
Rutgers University, New Brunswick, N.J. 08903

E.B. Brucker and E.L. Koller
Stevens Institute of Technology, Hoboken, N.J. 07030

W.M. Bugg, G.T. Condo, T. Handler and E.L. Hart
University of Tennessee, Knoxville, TN 37916

T. Kitagaki, S. Tanaka, H. Yuta, K. Abe, K. Hasegawa, A. Yamaguchi,
K. Tamai and T. Hayashino
Tohoku University, Sendai, Japan

R. Beringer, P. Cooper, S. Dhawan, H. Kraybill, R. Majka, P. McBride,
J. Sandweiss, A.J. Slaughter, H. Taft, L. Teig and L. Tzeng
Yale University, New Haven, CN 06520

TABLE OF CONTENTS

A PROPOSAL TO STUDY THE PROPERTIES OF HEAVY QUARK PRODUCTION AND DECAY

Proposal Summary

We propose to study the hadronic production, and subsequent decay, of states containing heavy quarks by using a high resolution, high rate, visual vertex detector in conjunction with a comprehensive downstream multiparticle spectrometer, the Heavy Quark Spectrometer (HQS).

We believe that the field of heavy quark physics, when studied with high resolution and high sensitivity, has great promise for new physics both for the study of the c and b quarks and τ lepton as well as for the search for new, unexpected phenomena. In addition, we believe that a major program of research, such as is proposed here, must be both flexible and comprehensive. For this reason, we propose to build the HQS as an "open-geometry" multiparticle spectrometer to take advantage of the variety of decay modes expected for heavy quark states. While a final design effort is still underway, we expect the HQS to contain the following elements:

(1) a high energy, high p_T muon trigger will be achieved by tracking a muon through an iron range absorber. Multimuon triggers also appear to be promising;
(2) the use of high resolution, visual vertex detectors (a high resolution streamer chamber and a microsonic bubble chamber) eliminates much of the combinatorial background which is a serious limitation to all other effective mass studies of heavy quark states. Additional resolution is expected through the use of holographic imaging of the tracks;
(3) a high field ($\sim$ 2T) magnet allows the detection of charged particles including those associated with the heavy quark non-hadronic decay which provides the trigger as well as those from the subsequent decay of the other associated heavy quark;
(4) the open geometry provides a maximal geometric acceptance for K°_S and Λ decays;
(5) two atmospheric pressure Cerenkov counters and a lead/scintillator sandwich shower detector provide the identification of particles from the heavy quark decays.

The direct observation of large numbers of B events ($\sim$2000) and charm decays ($\sim$100,000), as could be obtained in the program proposed here, would allow the following studies:

(1) determination of the Kobayashi-Maskawa parameters from measurements of lifetimes and branching ratios;
(2) confirmation that the b quark does have conventional weak couplings as expected if it is the q = -1/3 partner in a third left-handed quark doublet;
(3) study of the lifetime and decay modes of the τ lepton;
(4) possibility of observing CP violation in both neutral and charged B systems;
(5) the spectroscopy of the b (and c) states can be examined; and
(6) study the hadronic production mechanisms for both b and c quark states.

In addition to the above studies, it is important to note that the HQS, with its anticipated sensitivity and resolution, is ideally suited to search for new, unexpected phenomena in hadronic reactions. The high resolution of the visual detectors should permit the study of short-lived states with lifetimes $\gtrsim 1.4\times10^{-14}$ sec. The high sensitivity ($\sim$1 event/25pb) of these devices will allow the study of new and rare processes.

For this initial phase, we request 1000 hours of running with the streamer chamber and 1000 hours of running with the microsonic detector. We propose to run with proton beams at 400, 600 and 800 GeV and a π^- beam at $\sim$500 GeV with beam rates of 10^6-10^7/sec.

A PROPOSAL TO STUDY THE PROPERTIES OF HEAVY QUARK PRODUCTION AND DECAY

I. Introduction

We propose to use high resolution vertex detectors--both a high pressure, high resolution Streamer Chamber (HRSC) and a Microsonic Bubble Chamber (MSD)--and an open-geometry spectrometer with associated charged particle identification, electromagnetic shower detector, and muon detector to study the hadronic production and subsequent decay of particles containing the b quark.

The collaboration listed on the title page has been formed because of the common belief that the study of short-lived particles can best be performed using a high resolution ($\lesssim 30\ \mu$) visual detector with high-rate capability in front of a comprehensive downstream multiparticle spectrometer. Thus, this collaboration proposes to build the two vertex detectors and a downstream multiparticle spectrometer, the Heavy Quark Spectrometer (HQS). These two vertex detectors have complementary properties. The streamer chamber has excellent sensitivity but may be limited to track widths of 20-30 μm. The MSD, on the other hand, has limited sensitivity but offers the potential for tracks of width 2 to 5 μm. In the program proposed here, we have tried to utilize these complementary aspects in an optimum manner.

We believe that for an experiment that proposes to search for heavy quark decays with a starting date $\sim$ 1983, the system must be both flexible and comprehensive. For this reason we have proposed to build an "open-geometry" spectrometer which contains the following features:

i) measurement of charged particle momenta;
ii) identification of a large fraction of the produced $\pi^{\pm}$ and $K^{\pm}$;
iii) possibility of observing K°_{S} and Λ decays;
iv) γ, π° and electron detection and energy measurement; and
v) good muon identification.

We believe that all of these features are available in the system proposed in Section III.

In this experimental program we propose to use a high resolution vertex detector and the downstream spectrometer (HQS) to study the following physics topics related to the hadronic production and subsequent decay of B mesons and baryons:

a) a study of the production differential and total cross sections with high geometric acceptance;

b) a direct measurement separately of the lifetimes for the different charged and neutral B states by observation of both production and decay vertices in a visual detector;

c) since the trigger will involve only the decay of one b quark, we will study the inclusive decay modes of the other b quark; hence we can measure various branching ratios (e.g. nonleptonic, semileptonic,etc.) in an unbiased manner;

d) a study of the mass spectroscopy of the B systems by means of the effective mass technique, but without the usual combinatorial prolems associated with non-visual detectors; and

e) a search for and the measurement of CP violation in B decays.

In the following section, these and other topics are discussed in more detail.

The program of physics which can be carried out with the system we propose is a broad one which can develop along many lines, some of which we can forsee now and others which will become apparent only after the research gets underway. It is unreasonable to propose, at this time, all of the potential physics which could be done with the apparatus.

We have therefore planned, and proposed here, an initial phase which requests 2000 hours to survey the production properties of the B particles, to collect a substantial number of B events ($\sim$ 2000) and to collect a large sample ($\sim$ 100,000) of charm decays. Proposals for subsequent experiments would follow after this initial phase was at least partly completed.

Finally, we note that we are in the early stage of the design of the downstream system. The design, and costs, presented here are a "first-cut" in which we have tried to address the "large" questions in the design of such a system and to set the scale of the required apparatus. We are in the process of making a much more complete design effort, including an attempt to minimize costs. This is a substantial effort which will continue for some months. We do believe, however, that the design we have presented here will turn out to be representative of our "final" design and that it does reasonably display the scale of the equipment needed.

II. Physics Goals

In this section we discuss some of the outstanding questions that currently need to be answered concerning the nature of B production and decay. In addition, we indicate what information this experiment could provide to

answer some of these questions. Information from studies of the B can be generally classified into one of three categories:

(a) Production Mechanisms (Strong Interaction Physics),

(b) Decay Processes and Rates (Weak Interaction Physics), and

(c) Spectroscopy of heavy quarks.

(a) Production Mechanisms

i) Total B production cross section: From measurements of $B\bar{B}$ production by different beams (p, n, $\pi^{\pm}$, and $\bar{p}$), one will learn about the relative contributions of the $q\bar{q}$ and gg fusion diagrams (see Fig.1). While one "knows" what to expect from these two processes from studies of ψ production, it will be important to confirm these expectations directly. In particular, the overall normalization of the cross section could yield information on how the color-octet $q\bar{q}$ configuration rearranges itself by soft-gluon emission into a color-singlet final state.[1] In addition, these studies will provide necessary input for the subsequent choice of running conditions for future studies of heavy quark physics.

ii) Feynman x_F and p_T distributions: These studies can yield more detailed information on the relative contributions of the $q\bar{q}$ and gg mechanisms. Furthermore, depending upon the specific final state observed one can even study the various diagrams, eg., Fig.1 (b,c, and d). Small discrepancies between data and theory might enable one to learn about diagrams Fig.1 (e and f). In addition, one might learn about the heavy quark distributions in hadrons (see Ref.2).

iii) Diffractive Production: This process has been studied in charm production, but even here the picture is far from clear[3], and there have been no theoretical predictions for the diffractive hadronic production of B mesons or baryons.

(b) Decay Processes and Rates

Most of the items considered below apply to all of the B-mesons and baryons but will be discussed only for the mesons as examples of what might be studied. In addition, what is learned from e^+e^- machines in the next couple of years may well modify any trigger rates that are estimated for this experiment.

i) Lifetime of the B-Mesons (B_d°, B_u^-, B_c^-, B_s°,...): This is a study that will not be made at e^+e^- machines. Knowledge of the lifetime of the B's will yield approximate information on the value of the elements (and hence angles) of the Kobayashi-Maskawa (KM) matrix (see Appendix I).

ii) Lifetime of the τ-Lepton: From studies of $B \to \tau\nu$, $B^* \to \tau\nu$ or $F^-(\bar{c}s) \to \tau^-\nu$, etc., one could study the τ decay length distribution in a high resolution vertex detector and therefore measure the τ lifetime. An estimate of the τ lifetime is 2.7×10^{-13} sec.[4] In addition to its lifetime, if one sees the τ decay in the vertex detector one can also[4]:

a) determine whether the τ and μ couplings are the same;

b) look for the $\tau^- \to \nu K^-$ decay mode;

c) study the multihadron decay modes of the τ; and

d) set limits on forbidden decay modes., eg. $\tau^- \to \mu^-\gamma$.

iii) Specific decay rates: From studies of B-meson decay rates one can obtain information on the θ_i, δ KM parameters of Eq (AI-1). Since these parameters govern the lifetimes, decay branching ratios, mixing, and CP nonconservation of heavy quark systems, it is of considerable interest to determine them and the best way may be from studies of B-meson decay. The most likely key to measuring U_{bu} and U_{bc} (the amplitudes for $b \to u$ and $b \to c$, respectively) is through a study of multileptons from B decay. One could hope to measure $\Gamma(b \to u)/\Gamma(b \to c)$ by using the like-sign dilepton events from the cascade:[5-8]

iv) Non-Leptonic Enhancement Factors: Knowledge of the values of the KM angles is probably necessary in order to extract dynamical enhancement factors from B lifetime measurements. In principle,[9] with measurements of the ratios $\Gamma_{SL}(b \to u)/\Gamma_{NL}(b \to u)$ and $\Gamma_{SL}(b \to c)/\Gamma_{NL}(b \to c)$ we can measure the dynamical nonleptonic enhancements without knowing the KM angles; however, this is likely to be hard and probably will be easier if the KM angles are known.[9]

v) Color Rearrangement in Non-Leptonic Decays: Measurement of the $B \to \psi X$ decay will yield information on the dynamics of the non-leptonic decays. Depending upon how (or if) the color-octet $c\bar{c}$ system emits soft gluons to become an observable color singlet final state, there is a factor of 9 uncertainty in the calculated rate for B decays into $c\bar{c}$ bound states.

vi) Tests of the b Spin: A suggestion[10] has been made to search for effects that could indicate that the b quark has spin 3/2 rather than 1/2. If $s_b = 3/2$ and $s_{u,d} = 1/2$, then the lowest-lying mesons in the B system stable against strong and electromagnetic decays will be spin 1, not spin 0 as for charm. Furthermore, b decays could occur via flavor changing neutral spin 0 or 2 mesons.

Kane and Raby emphasize that if a spin 3/2 b quark were to be found, we would have to consider seriously the possibility that quarks and leptons were made of more elementary objects.

vii) Measurement of the weak decay constant for B mesons: Measurement of the branching ratio for $B^- \to \tau^-\nu$ would give direct information on f_B. Even though this mode is relatively small (0.4 - 4%), it could be studied in this experiment. Several calculations[11] yield the expectation that $f_B \sim 500$ MeV. However, another estimate[12] based on the MIT bag model predicts $f_B \sim 50$-70 MeV. Thus, a measurement of f_B through leptonic B decays could yield information about the hadronic structure of the charged B mesons.

viii) Evidence for "Penguin" graphs: Guberina et al[13] have suggested that it would be good to look for the effects of penguin graphs in a nonleptonic multibody channel. Specifically, they suggest looking at the two and four-body decays $B^- \to \pi^-\bar{K}^\circ$, $\pi^-\pi^\circ$ or $B \to K3\pi$, 4π. According to their analysis they expect that $B \to \pi K(B \to K3\pi)$ should be similar to the rate for $B \to 2\pi(B \to 4\pi)$, in contrast to the naive predictions of the KM model (see Eq. AI-3). (Indirect production of $K3\pi$ coming from $B \to D\pi \to K3\pi$ or $B \to D\pi\pi \to K3\pi$ should be comparable but can be isolated by studying the effective mass distributions for the D contribution.)

ix) Flavor-changing neutral currents: If τ's are made at reasonable rates at Tevatron energies via B (and/or F) decays, than the search for the reactions $\tau \to \mu\mu e$ or eee would set limits on flavor-changing neutral currents.[14] It will be impossible to approach the limit suggested[14] by K° data of $B(\tau \to \mu\mu e) < 5 \times 10^{-10}$; but even a limit of 10^{-3} might be useful since no directly measured limit exists at present.

x) CP Violation Studies: For only four quarks (two weak isospin left-handed doublets), any complex phase parameter in the weak currents can be transformed away by a redefinition of the quark fields. Thus, in the absence of further interactions, there is no CP violation. For the case of six quarks this is no longer true and the phase parameter δ appears (see Eq. AI-1). Consequently, there is CP violation if δ differs from zero.

Now consider $B^\circ\bar{B}^\circ$ production followed by the semileptonic decays $B^\circ \to \ell^- \nu X^+$, $\bar{B}^\circ \to \ell^+ \bar{\nu} X^-$. CP violation appears as a charge asymmetry in the number of like-sign dilepton events: $a = (N^{++} - N^{--})/(N^{++} + N^{--})$. Since $A = (N^{++} + N^{--})/2N^{+-} \simeq 0.4$, we see [15-18] that charge asymmetries could be large in $B^\circ - \bar{B}^\circ$ decays: $|a| \sim 4 \times 10^{-4}$ ($\sim 4 \times 10^{-3}$) for B_d (B_s). Given the large value of A, such values of $|a|$ could be observed with a large number of dilepton B° events. Furthermore, the analysis of Ref. 15 suggest that $a < 0$. Hence, if large lepton charge asymmetries in excess of 10^{-2}, or in the direction of (++) rather than (--), were to be observed, this would be evidence for an alternate means of CP violation.

The above CP violation effects occur due to virtual (off-shell) mixing effects in their mass and width matrices. Recent studies[19-20] have shown that it may be better to look for CP violation in processes where CP violation is coming mostly (for B°) or completely (for $B^\pm$) from on-shell transitions in the decay amplitudes[21]. Although the CPT theorem guarantees that the total widths of particle and anti-particle are identical, one prediction[19] of CP violation is that the decay rate of a particle into a definite final state can differ from the rate of the antiparticle decaying into the corresponding charged-conjugated state: $\Gamma(i \to f) \neq \Gamma(\bar{i} \to \bar{f})$. Such differences,

if observed, would yield the first evidence for time-reversal violation involving non-neutral systems[19]. Thus one should look for asymmetries between particle-antiparticle decay rates such as

$$\frac{\Gamma(B \to DX) - \Gamma(\bar{B} \to \bar{D}X)}{\Gamma(B \to DX) + \Gamma(\bar{B} \to \bar{D}X)} \quad .$$

Three types of studies have been suggested [19,20]. In the first type[19] one can study asymmetries in either partial widths or inclusive decays of the charged $B^{\pm}$ mesons ($B_u^{\pm}$ and $B_c^{\pm}$):

$$B_u^{\pm} \to \pi^{\pm}\pi^{\circ} \ , \ K^{\pm}\pi^{\circ}$$

$$B^{+} \to \pi^{\pm}X \text{ vs } B^{-} \to \pi^{\mp}X.$$

The second type involves producing, through mixing, a coherent beam of B° and $\bar{B}^{\circ}$ and observing a decay channel to which both components contribute:

$$B^{\circ} \to D^{\circ}X \to K_s^{\circ}YX \text{ with rate } \Gamma$$

$$\bar{B}^{\circ} \to D^{\circ}X \to K_s^{\circ}YX \text{ with rate } \bar{\Gamma} \ ,$$

or the processes

$$B_d^{\circ}\bar{B}_d^{\circ} \to K^{+}K_s^{\circ} \ X^{-} \quad \text{with rate } \Gamma$$

$$\to K^{-}K_s^{\circ} \ X^{+} \quad \text{with rate } \bar{\Gamma} \ .$$

For the latter reactions, Carter and Sanda [20] conclude that $a = (\Gamma-\bar{\Gamma})/(\Gamma+\bar{\Gamma}) \sim$ few % and thus might be observed in future high statistics experiments. Finally, they stress the importance of observing hadronic (as opposed to semileptonic) final states and, in particular, those final states containing K_s°.

The third type of study involves the interference between $B^{-} \to DK_s^{\circ}X$ and $B^{-} \to \bar{D}K_s^{\circ}X$ if a common decay channel $K_s^{\circ}K_s^{\circ}Y$ is detected.

xi) Evidence for eight or more quarks: Since the charged-current matrix must be unitary, knowledge of the KM angles might enable one to look for evidence of more than 6 quarks. The presence of new quarks leads[22] to the deviation of the matrix from unitarity, with their contribution being $\sim 1/\sqrt{m_q}$.

xii) Evidence for the conventional six-quark model: Most discussions assume that the b quark is the q = -1/3 partner to a third quark doublet. While the e^+e^- data from CESR [23] seem to suggest that the b quark does have conventional weak couplings [24], it is still important to check that the properties of the b are inconsistent with other theories in which there is no t quark [24]. As an example, Barger and Pakvasa [25] have considered the consequence of assigning the b quark to a left-handed singlet rather than to the weak isospin doublet $(t,b)_L$. In this case, no higher mass t quark would be required. Distinctive tests of a singlet assignment would be the neutral current modes with the following signatures:

	$b \to se^+e^-$ (2%)	observed as	$B \to Ke^+e^-$, $K\pi e^+e^-$, ...
	$b \to s\mu^+\mu^-$ (2%)		$B \to K\mu^+\mu^-$, $K\pi\mu^+\mu^-$, ...
	$b \to s\nu\bar{\nu}$ (12%)		$B \to K$ + missing energy
or	$b \to de^+e^-$ (1%)		$B \to \pi e^+e^-$, etc.

The existence of a t quark can be established by ruling out these decay modes at this level [26]. Note that both PETRA [26] and CESR data may be close to doing this, with $B(B \to e^+e^-X)<5\%$ and $B(B \to \mu^+\mu^-X)<1.7\%$ (90% C.L.) for CLEO data [27]. Another decay mode of interest is

$$b \to s\bar{s}s \quad (3\%)$$

with an additional 6% $s\bar{s}s$ contribution from $b \to c\bar{c}s$ and $c\bar{c}c$. Hence the total $s\bar{s}s$ contribution is almost double that expected in the KM $(t,b)_L$ doublet model. This is particularly interesting in view of the excess of K's observed experimentally at CESR [23].

(c) Spectroscopy of Heavy Quarks

Any study of B mesons will certainly include a study of the mass spectroscopy of the b quark. While the first states are likely to be found in e^+e^- experiments, it is quite likely that there are many states which are not produced in e^+e^- reactions or states which are difficult to detect in a colliding beam experiment. Clearly, any experiment which can trigger effectively on b decays and detect the decay vertex in a visual detector will have a great advantage in eliminating from an effective mass calculation those particles which do not come from the decay vertex. Thus the hadronic decays of b states ($\sim$ 69% of the decays are non-leptonic) will permit a clean study of both mesons and baryons containing the b quark.

(d) How do we tell B from charm?

Since it appears that the easiest trigger for a B search experiment will involve one or more detected leptons (e,μ), it will be important to "remove" as much of the "charm background" as possible. In this section we consider some of the characteristic features of $b\bar{b}$ production and decay.

i) One can search for the observation of two distinct short-lived decays in an event in which an identified muon, produced in the event, does not come from either of the two distinct decays. Events of this type will "signature" B production even if the B lifetime is too short to observe as a clearly distinct vertex in the vertex detector. The efficiency for such events will be high for our experiment because we will have excellent resolution for charm detection, B's are known to largely decay via charm and our trigger responds mainly to the muon from the $B(\bar{B})$.

ii) Two-kink Tracks: Following a trigger, one can scan the pictures from a visual detector and look for tracks which contain two sequential kinks. This does not guarantee B production and decay:

$$b \to c + X,$$
$$\quad\; \lfloor\!\!\rightarrow s + X$$

since one could also have rare charm processes such as

$$F \to \tau + X.$$
$$\quad\; \lfloor\!\!\rightarrow \mu + X$$

However, even these processes are of interest, and furthermore, some of the two lepton triggers can be used to suppress this process.

iii) Effective Mass Combinations: If a single decay vertex has been located in a picture, the combinatorial problems associated with the usual effective mass plots in high multiplicity events will be greatly reduced. Since one will "see" which charged tracks emerge from the decay vertex (with maybe a single ambiguity depending upon how well one can match tracks detected downstream with the tracks observed in the visual detector), the effective mass calculation need only include those charged particles. In general, there will still be some ambiguity in assigning the detected π^0's and K^0_S's, but the problem will be greatly

reduced over experiments which do not "see" the decay vertex.

iv) Exotic decays of $b\bar{b}$: Despite the factor of 10^3 in the ratio of production cross sections for $c\bar{c}$ to $b\bar{b}$ ($s\bar{s}$ occurs in 5×10^{-2} of all interactions, $c\bar{c}$ in 10^{-3} and $b\bar{b}$ in 10^{-6}), there are various exotic final states which clearly signal b-quark production. While all of these rates are quite small, they may still be of use either incorporated as a trigger (eg., the multilepton final states) or in the off-line analysis (eg., the multi-strange final states). In particular, the trigger will be extremely important to suppress "charm background" for B studies.

v) Multilepton final states: In Appendix II we consider the various multilepton final states that are possible from $B\bar{B}$ decay. The most important results, and ones which will be used in the trigger and event calculations below, are the following:

a) $\geq 1\mu$(or e) = 0.40

b) $\geq 2\mu$(2e, or μe) = 0.040

c) $B \to \psi \to 2\mu$(or 2e) = 0.0028

d) $B \to \tau^- \to \mu^-$(or e^-) = 0.01.

III. Experimental Apparatus

The layout of the proposed downstream detector is shown in Figure 2. In this section we discuss each of the components.

(a) Beam

Since we believe that a detailed study of B production should include a comparison of $B\bar{B}$ production by both mesons and nucleons, we request high intensity π^- and proton beams. For this proposal we have assumed a 10 second pulse every 60 seconds at the Tevatron. As discussed in Section V, we propose to begin our program with proton beams of $\sim 10^7$ per second (or 10^8 per 10 sec Tevatron flat top), and with π^- beams of 10^6 per sec (10^7 per pulse). However, we expect to require more intense beams in the later stages of the program. In particular a proton beam of 10^8 per second (10^9 per pulse) or a neutron beam of similar intensity will be essential for the very large statistics runs to study special aspects such as CP violation. The beam optics should be such that all beams can be designed to fill the sensitive area of the vertex detector, the largest of which is the HRSC with dimensions 10cm x 1cm (and 20cm in the beam direction). The MSD will require a finely focussed beam of dimensions 3cm x 2mm. Finally, we note that for the charged particle beams, we will

build a pair of beam tagging hodoscopes (H_a,H_b) to measure the direction of the beam for use in triggering for the "low" intensity beam cases.

(b) Vertex Detector

The visual vertex detector proposed for this experiment is described in detail in Appendix IV.

(c) Magnet

We request a magnet 1.2m wide and 0.6m gap. The magnet should be 2m in the beam direction and be capable of producing a 2T central field.

(d) Proportional Multiwire Chambers

Directly following the vertex detector, we propose to place two PWC triplets P_1,P_2. Inside the magnet volume, we propose to use 5 PWC triplets P_3-P_7. The properties of all of these chambers are given in Table I.

Table I

Proportional Wire Chamber Characteristics

PWC Triplet	Width x Height	Spacing Vertical, ± 30°	Total Wires
P_1,P_2	0.6m x 0.3m	1mm, 2mm	2600
P_3-P_7	1.2m x 0.6m	2mm, 3mm	7600
P_8-P_{12}	2.0m x 1.6m	3mm, 3mm	11050
			21250

Downstream of the magnet, we propose to use 5 large PWC's also described in Table I. The first two of these planes, P_8 and P_9, are used to provide tracking of particles after the magnet, through the two Cerenkov counters and into the shower detector. The last three triplets, P_{10}-P_{12}, are used to track the muon through the steel absorber and will be discussed later in connection with muon identification.

(e) Cerenkov Detectors

As we have seen, we expect that most B decays will occur via charm and hence yield strange particle final states. In Section IV, we present the momentum spectra for the K's and note that it ranges from approximately 5-50 GeV/c (see Figure 3). In order to identify as many $K^{\pm}$ as possible, we propose to use two Cerenkov counters with the following properties:

Table II

Cerenkov Counter Characteristics

Cerenkov	Dimensions long x wide x high	Number of Cells	Gas	Thresholds p K π	Max Radius
C_1	2.5m x 2m x 1.0m	28	CO_2	33 17 5	7.1cm
C_2	4.0m x 2m x 1.6m	28	Ne	82 43 12	4.5cm

The maximum number of photoelectrons expected, assuming a figure of merit of $A=100cm^{-1}$ (note that a neon counter has achieved $A=260cm^{-1}$, see Ref. 54), are 20 and 5 respectively. In addition, behind each Cerenkov counter, we place a hodoscope (H_1,H_2) which matches the sizes of the mirrors in each counter.

(f) Electromagnetic Shower Detector

Our preliminary design for a shower detector has dimensions of 2.4m (wide x 1.6m (high) and is located 10m downstream of target center. It is designed to meet the demands of 1) a good e/π separation in the momentum range 5-50 GeV/c, and 2) detection of π°'s in the 10-50 GeV/c range. The shower detector is of a lead/acrylic scintillator sandwich construction, with a total depth of approximately 20 radiation lengths (r.l.), sufficient for total absorption of showers up to 50 GeV/c. (55)

The shower detector forms an array made of 32 modules. Each module has a sensitive area of 240cm x 5cm and consists of 32 identical layers, each of which has 1/8" (0.6 r.l.) of lead followed by 1/4" of plexipop, yielding a total of approximately 20 r.l. The energy resolution to be expected from this type of shower counter is given by (56)

$$\frac{\sigma_\bullet}{E} \sim \frac{12\%}{\sqrt{E}}$$

Each module is read out by means of wave shifter at both ends. Thus the longitudinal position along the length of a module is determined by comparing the relative pulse heights and timing information of the two corresponding photomultipliers. A resolution of ± 2cm has been reported in a similar device (57). A further improvement in position as well as in e/π separation is to be achieved by inserting two wire chambers with 1cm wide cathode strip readout in each module at a depth of 3 and 7 r.l. respectively.

With good energy and spatial resolution of the shower detector, combined with a good momentum resolution in the magnetic tracking system, we expect a pion rejection ratio in excess of 10^3 at 10 GeV and about 5×10^3 at 30 GeV with a loss of only 5-10% of the electrons.

For identifying π^o's, the minimum separation (at 10.0m) between two photons is (E in GeV) $d \sim 270\text{cm}/E$. Hence, with a conservative resolution of $\sigma \sim 2$cm, π^o's of energy 50 GeV ($d \sim 5.4$cm) can be readily identified.

(g) Muon Identification

The expected trigger for this experiment will be a single muon with momentum greater than 10 GeV/c and with a transverse momentum $\gtrsim 1.5$ GeV/c. We expect to use a range absorber (7.3m of Fe) to select muons above the minimum momentum. To select the transverse momentum trigger, we propose to insert three large PWC's (P_{10}-P_{12}) after 4m, 5m and 6m of steel. The 4m position is selected in order to cut the particle rate from π, K punch-through to a reasonable value. The other locations are chosen to provide adequate position measurement to select muons coming from the vertex detector (in the non-bending direction) and the measurement of the momentum and angle (in the bending direction). The final element in the muon detector is a 20 cell hodoscope (H_3) which is used to trigger the system and to provide the additional trigger logic of multimuons (either of like-sign or of opposite sign) by selecting various patterns of hits.

(h) Trigger Processor

Because of the memory time of the visual vertex detector, we must make a trigger decision in about 1μsec. The technique that we are presently considering is an asynchronous parallel processor based upon multiple fast memory lookups (MLU). Such a system has been designed by Barsotti et al [58] and is currently used in E516, with a second such system currently being installed in E-537. A single MLU takes 35-50 nsec in this system with each lookup beginning as soon as the input data (address) is available. High speed is attained by using multiple MLU's in parallel so as, for example, to calculate x and y track parameters at the same time. Designing the chamber placement and readout to facilitate the trigger calculation, an MLU trigger processor should give a muon trigger cut on both P_μ and P_T in 1μsec or less.

IV. Acceptances and Trigger Rates

The triggers selected for this experiment will be one or more leptons. The simplest trigger is the detection of a high transverse momentum ($p_T \gtrsim$ 1.5 GeV/c), high momentum (p > 10 GeV/c) muon. In order to calculate the rates that we can expect, we have performed Monte Carlo calculations for the following sources of high P_T muons:

a) Background due to $\pi^{\pm}$, $K^{\pm}$ decays;

b) $D\bar{D}$ production, followed by $D \to K\mu\nu$, $K^*\mu\nu$ decays; and

c) the signal from $B\bar{B}$ production, followed by

$$B \to \mu\nu D\ (n\pi),\ D\ (m\pi)$$
$$\hookrightarrow K\mu\nu,\ K^*\mu\nu.$$

a) Background from $\pi^{\pm}$, $K^{\pm}$:

We parameterize the $\pi^{\pm}$ ($K^{\pm}$) production spectra following B. Alper et al[28] at 800 GeV/c ($\sqrt{s}$ = 39 GeV):

$$\frac{dN}{dydp_T} = p_T e^{-Ap_T} e^{-By^2}$$

where A = 7.5 (4.6)$(GeV/c)^{-1}$ and B = 0.205 (1.39) with an average number of $\pi^+ + \pi^-$ = 10.4 per event, and an average number of $K^+ + K^-$ = 0.56/event. Including a $K \to \mu$ branching ratio of 0.63%, this yields 0.36 ($K \to \mu$)/event.

b) Background from $D\bar{D}$ production:

Following A. Diamant-Berger et al [29], we parameterize the $D\bar{D}$ spectra as

$$\frac{dN}{dMdxdp_T} = \frac{1}{M^3} p_T e^{-cp_T} (1-|x|)^n e^{-dM/\sqrt{s}}, \qquad (1)$$

where c = 1.3 $(GeV/c)^{-1}$, n = 6 and d = 20, M ($\geq$ 3.8 GeV) is the mass of the $D\bar{D}$ pair and x, p_T refer to the M system which then decays into $D\bar{D}$ isotropically. The two D - mesons are then allowed to decay into[30] $K\mu\nu$ (with B.R. = 0.59x0.082) and $K^*\mu\nu$ (B.R. = 0.41x0.082) with a phase space distribution.

c) Signal from $B\bar{B}$ production:

The production of $B\bar{B}$ events was also parameterized by equation (1) with c = 2.2 $(GeV/c)^{-1}$, n = 3 and d = 15. Data from CLEO[32] show that the observed charged particle multiplicity for $B\bar{B}$ decays agrees well with a Monte Carlo calculation when $\langle n_c(B\bar{B}) \rangle$ = 11.8 ± 1.0 is used. Hence we find $\langle n_c(B) \rangle$ = 5.9 ±0.5 or correcting for neutrals $\langle n(B) \rangle$ = 1.5 x 5.9 = 9 ± 0.8. Therefore we allow the B to decay into an average of 9 particles.

Since most B decays are expected to occur via b → c (see Appendix I), we have considered the following sources of muons:

$$B \to D\mu\nu\ (4\pi); \tag{2}$$

$$\to (\mu)\ D\nu\ (4\pi); \text{ and} \tag{3}$$
$$\quad \hookrightarrow K\mu\nu,\ K^*\mu\nu$$

$$\to D\ (7\pi)\ . \tag{4}$$
$$\quad \hookrightarrow K\mu\nu,\ K^*\mu\nu$$

Since there are some indications[27] that semi-leptonic B decays may occur through $\mu\nu D$ and $\mu\nu D^*$ (2000), we have also considered the decay

$$B \to D\mu\nu\ . \tag{5}$$

Using reaction (5) rather than reaction (2), increases the acceptance for single muons from B decay by ∿ 10%. For the remainder of this proposal, however, we just use reactions (2)-(4).

d) Production Cross Sections

We have assumed the following cross sections:

$\sigma\ (NN)_{inel} = 41 - 7 = 34$ mb,
$\sigma\ (D\bar{D}) = 50$ μb, and
$\sigma\ (B\bar{B}) = 50$ nb .

Justification for the last value is given in Appendix III.

e) Acceptance Results

Using the downstream system, with the given dimensions as discussed in III, the results for the reactions (2)-(4) are shown in Fig 4 as a function of the minimum value of the muon p_T that we accept. A minimum momentum cut of 10 GeV/c has been applied. The results are presented in terms of the acceptance times expected branching ratio for production of a μ in B decay. The upper curve in Fig 4 shows the sum of the three lower curves.

As we have seen in Section II, many of the B decay channels yield K meson final states. Using the two Cerenkov counters discussed in Section III and reactions (2) and (4), we show in Fig 3 the momentum spectrum for $K^{\pm}$ that strike the mirrors of both Cerenkov detectors. As shown, the overall acceptance for each reaction is about 80%. (The acceptance for K's from

$D\bar{D} \rightarrow K$ is greater than 90%, not shown).

The trigger rates, expressed as the number of triggers per NN interaction, are shown in Figure 5 as a function of the cut on P_T of the muon. We note that background μ's from $\pi^{\pm}$ decay are negligible compared to $K^{\pm}$ decays. The trigger rates from $D\bar{D}$ production are a factor of 100-200 greater than the rate from $B\bar{B}$ production.

In the charm rate calculations to be presented in Section V we have used the charm production cross sections calculated by Afek et al.[59] These are low by a factor of two at 800 GeV/c incident momentum in comparison with the 50μb used in the trigger calculation above. We have taken the conservative point of view of using the larger charm cross section when calculating background triggers for B production and the lower charm cross section when calculating yields of charm events for physics studies. We have used the Afek et al. [59] calculation because it provides a consistent prediction of charm cross sections for the full range of incident beam energies we propose to study.

The actual value of the transverse momentum cutoff which will be used will be determined after considerable experimental as well as "theoretical" study. A key consideration will be the trade-off between trigger acceptance and trigger rejection rate. A proposed program for the first phase of our experiment is given in Section V. We present in Table III the principal parameters of the proposed HRSC and MSD which enter into the rate calculations of Section V.

Table III

PARAMETERS OF PROPOSED HRSC

Gas	Ne/He @ 100 atmospheres or equivalent
Dimensions of visible region	20 cm x 10 cm x 1 cm
Fiducial length	20 cm
Fiducial interaction probability per incident nucleon	.0118
Non-fiducial interaction probability per incident nucleon (dead gas, windows, upstream, etc.)	.0066
TOTAL	.0184
Chamber dead time per picture	50 ms
Track width (space)	20-30 μm.

PARAMETERS OF PROPOSED MSD

Liquid Composition	Freon (CF_3Br)
Dimensions of visible region	10 cm diameter x 0.36 cm deep
Fiducial length in beam direction	8 cm
Fiducial interaction probability	0.1
Non-fiducial interaction probability	0.025
TOTAL	.125
Chamber cycling rate	10^4 HZ
Track width (space)	2-5 μm

V. Proposed Program

The system we are proposing will have a broad capability for the study of heavy quark physics. We envision an experimental program with this system which will encompass many different aspects of the physics, many different experimental runs and, undoubtedly, other experimenters besides those listed on this proposal.

We propose to start this program with an initial "survey" phase which will give the necessary information for the choice of future experiments as well as providing answers to some of the "first order questions" of b quark physics, and provide a large ($\gtrsim$ 70,000) sample of charm decays.

The details and rationale for this initial phase are given below. Subsequent experiments with the system will be the subject of future proposals.

The HRSC, with its high sensitivity, is the instrument of choice for measuring the B particle production cross sections. It is important to note that in the system we propose, B particle production can be identified with high efficiency even if the lifetime of the B particles is too short to observe directly in the HRSC. This is because the HRSC will have excellent efficiency ($\gtrsim$ 90%) for charm, and, with our triggering scheme -- one or more high transverse momentum muons (with $P_T \geq 1.5 - 2.0$) -- the "trigger" muon is almost always from a B particle, not from a daughter charmed particle.

In the event of a "short" B lifetime, a B production event will then appear as an event with two visible charmed particles in the chamber and with a muon which "comes from" the primary vertex. The identification of muon tracks in the HRSC will be done by matching the track direction with the direction of the muon(s) identified by the downstream system. Careful attention is being given to the system design to assure that this matching can be done to sufficient accuracy to make the identification of the muon track(s) in the HRSC essentially free of ambiguity.

Although we are still in the process of carrying out detailed Monte Carlo studies of direct observation of B particle decays in the HRSC and the MSD we have approximate estimates of expected efficiencies from the previous work of ourselves and others. Figure 6 shows the results of a detailed charm Monte Carlo carried out by the Rutherford group in the LEBC collaboration.[60] The detection efficiency for B's can be expected to be quite similar so that direct observation of B particles in the HRSC (track width 20-30 μm) will be $\gtrsim$ 50% efficient for $\tau_B \gtrsim 10^{-13}$ sec, and in the MSD (bubble diameter 2-5 μm) will be $\gtrsim$ 50% efficient for $\tau_B \gtrsim 1.5 \times 10^{-14}$ sec. Direct observation of charm will be highly efficient for both detectors.

Our strategy for the initial phase is then to use the HRSC to study B particle production with proton beams at three energies, 400 GeV, 600 GeV and the peak operating TEVATRON energy which we take, for this proposal, to be 800 GeV.

We also propose to use the HRSC to study B production by pions at the highest energy for which 10^6 pions per second (10^7 pions per 10 sec pulse) can be provided in the beam to the detector. We have estimated this pion energy to be 500 GeV for TEVATRON operation at 800 GeV.

The MSD would be used, in this proposal, to make a long run (1000 hours) at the peak energy, in a proton beam, to collect a sample of events with the maximum possible resolution. We have requested proton beam fluxes that correspond to 10 tracks per sensitive time (about 1 μs for both HRSC and MSD). The presence of 10 beam tracks in a picture is acceptable even with ordinary imaging optics. With holographic recording, an order of magnitude larger number of beam tracks per picture should be acceptable. For the "initial phase" we have, however, kept the maximum flux to the 10 per μs level, partly to be conservative on the photography and partly because this flux corresponds to 10 MHZ of beam passing through the downstream spectrometer. We will give careful consideration to the rate capability and beam "hardness" of the downstream spectrometer and it may well be that higher beam fluxes may be useable in future runs. We therefore request

that the beam line we use be such as to allow the use of proton fluxes up to 10^8 per second (10^9 per pulse).

We would expect to need a period of running time, somewhat hard to estimate now, to shake down the system and to study experimentally the various triggers. We estimate approximately 500 hours for this shakedown phase. This could largely be done at lower beam intensity. The actual, initial, data running conditions would of course be determined after these studies. We do believe, however, that we have a fairly good overall idea of the data phase running requirements. The tables below summarize our requests and expected yields for the start up and initial experimental phase of our proposed program. Typical calculations of the rates listed in the table are also given below.

Table IV

HQS - "Shakedown" Phase

Energy (GeV)	Particle	Incident Flux		Hours Requested	Comments
		Instantaneous	per pulse		
400-800 (as available)	P	$\geq 10^4$	$\geq 10^5$	400	General set-up, Timing, trigger Studies, etc.
800	P	10^7	10^8	100	Maximum rate Studies

Table VI HQS - B Particle Production Survey (HRSC)

Beam Particle	Energy (GeV)	Incident Flux		P_T min for Trigger (GeV/c)	Hours Requested	Total Pictures	Fiducial $B\bar{B}$ per pix		Total Fiducial $B\bar{B}$		Fiducial $D\bar{D}$ per pix		Total Fiducial $D\bar{D}$	
		Inst.	per pulse				$A^{2/3}$	A	$A^{2/3}$	A	$A^{2/3}$	A	$A^{2/3}$	A
P	800	10^7	10^8	2.0	400	2.9×10^5	$\frac{1}{303}$	$\frac{1}{113}$	959	2577	$\frac{1}{8.8}$	$\frac{1}{3.3}$	$.33\times10^5$	$.88\times10^5$
P	600	10^7	10^8	2.0	100	$.725\times10^5$	$\frac{1}{615}$	$\frac{1}{229}$	118	317	$\frac{1}{11.9}$	$\frac{1}{4.4}$	$.61\times10^4$	1.64×10^4
P	400	10^7	10^8	2.0	200	1.45×10^5	$\frac{1}{1954}$	$\frac{1}{727}$	74	200	$\frac{1}{15.9}$	$\frac{1}{5.9}$	$.92\times10^4$	2.46×10^4
π^-	500	10^6	10^7	1.5	300	1.35×10^5	$\frac{1}{3211}$	$\frac{1}{1195}$	42	113	$\frac{1}{27.9}$	$\frac{1}{10.4}$	4,820	1.30×10^4
Totals					1,000	6.425×10^5			1,193	3,207			53,120	142,000

Table VI HQS - Highest Resolution Study (MSD)

Beam Particle	Energy (GeV)	Incident Flux		P_T min for Trigger (GeV/c)	Hours Requested	Total Pictures	Fiducial $B\bar{B}$ per pix		Total Fiducial $B\bar{B}$		Fiducial $D\bar{D}$ per pix		Total Fiducial $D\bar{D}$	
		Inst.	per pulse				$A^{2/3}$	A	$A^{2/3}$	A	$A^{2/3}$	A	$A^{2/3}$	A
P	800	10^7	10^5	1.5	1000	3.17×10^5	$\frac{1}{230}$	$\frac{1}{272}$	433	1,165	14.8	5.5	2.14×10^4	5.76×10^4

As an example of the calculations used for tables V and VI we give below the details for the 800 GeV proton exposure of the HRSC.

From the table of chamber parameters in section IV:

Total interaction probability per incident proton for HRSC = .0184

Fraction of all interactions which are in fiducial region = $\frac{.0118}{.0184} = .64$

From figure 4 we see that the net probability of triggering on a $B\bar{B}$ production event by detecting one or more muons with $P_T \geq 2.0$ GeV/c (and as assumed throughout, $P_\mu \geq 10$ GeV/c) is 2.3×10^{-2}. From figure 5 we see that the total probability of triggering under these conditions is 7.0×10^{-6} per interaction and is largely due to charged K decays.

For 10^7 instantaneous beam rate the ungated trigger rate is N_u:

$$N_u = .0184 \times 7 \times 10^{-6} \times 10^7 = 1.288 \text{ sec}^{-1}$$

The gated trigger rate N_T is (recalling that chamber dead time is .05 sec.)

$$N_T = 1.288(1-.05N_T)$$

$$N_T = \frac{1.288}{1.0644} = 1.21 \text{ gated triggers/sec.}$$

Assuming, as before, that the TEVATRON produces a 10 sec pulse every 60 sec we now calculate the number of gated triggers (the number of pictures) in 400 calendar hours:

$$\text{No. of gated triggers in 400 hrs} = \frac{1.21}{6} \times 60\text{x}60\text{x}400 = 2.9\text{x}10^5$$

Taking the $A^{2/3}$ case, i.e., assuming that $B\bar{B}$ production scales with the A of the target nucleus as $A^{2/3}$, we now calculate the $B\bar{B}$ event yields in these pictures.

As noted in section IV, we assume the $B\bar{B}$ production cross section in nucleon-nucleon collision at 800 GeV incident energy is 50 nb. For the $A^{2/3}$ case, both $B\bar{B}$ and ordinary interactions

scale the same way with A, so f, the fraction of inelastic interactions producing $B\bar{B}$ is:

$$\text{Fraction of inelastic interactions producing } B\bar{B} = \frac{50\times10^{-9}}{31.8\times10^{-3}} = 1.57\times10^{-6}$$

(We have taken the p-p inelastic cross section to be 31.8 mb)

$$\text{The fraction of triggers containing } B\bar{B} \text{ in fiducial region} = \frac{1.57\times10^{-6}\times2.3\times10^{-2}\times.64}{7.0\times10^{-6}}$$

$$= 3.301\times10^{-3} = \frac{1}{302.8}$$

$$\text{The number of pictures in 400 hr run containing } B\bar{B} \text{ in fiducial region} = 2.9\times10^{5}\times3.301\times10^{-3}$$

$$= 957.3$$

The calculation, with the assumption that $B\bar{B}$ production scales like A of the target proceeds in a straightforward manner. We note for the 9/1, Ne/He gas of the HRSC:

$$\langle A^{2/3} \rangle = 6.88$$

$$\langle A \rangle = 18.4$$

Thus for the A assumption, $B\bar{B}$ trigger rates are enhanced ralative to the $A^{2/3}$ case by 18.4/6.88 = 2.7.

For D particle production, we use the $D\bar{D}$ trigger rate given in figure 7, scaled down by the ratio 24.8/50 because we assume the $D\bar{D}$ production cross section of Afek, et. al.[69] for physics rates and the flat 50 μb of $D\bar{D}$ for background trigger rates to $B\bar{B}$ events.

The expected yields for the lower energies are calculated assuming the calculations of Afek, et. al.[59] for the $B\bar{B}$ production cross section. For the pion incident beam, we have assumed the same cross section as for protons of the same energy.

VI. Analysis of Holograms

Since hundreds of thousands of holograms will be taken during this experiment, it is important that the scanning and measurement be quick, convenient, and accurate. Plans for the development of both equipment and software are already underway.

It appears that the equipment and programs will be comparable to and perhaps even simpler than was the case for analyzing normal bubble chamber photographs. This arises partly because of the experience gained with normal photographs. Further, since each hologram produces three dimensional images, tracks will not often cross one another, thereby decreasing the confusion and the difficulty of pattern recognition. The fact that all three dimensional information is on a single hologram instead of on three different rolls of film is a considerable advantage.

Before discussing specific hardware, we present a few general considerations. Let us assume the bubbles or streamers are 5 microns in diameter. Given an adequate image and a good stage, it should be possible to measure to 1 micron in a plane (X,Y) parallel to the plane of the hologram. The accuracy in the direction perpendicular to the plane of the hologram (Z) is not so obvious. It can easily be shown that:

$$\Delta s = Cs/D$$

where D = diameter of the effective area on the film,

C = diameter of circle of confusion in a real size image,

s = distance from film to object.

Δs = depth of focus = change of s from the position of perfect focus such that a point object produces a circular image of diameter C.

To get a feel for the possibilities, take s = 20 cm and D = 1 cm (reasonable numbers for the holograms from BIBC). For a scan mode at low magnification, where most or all of the chamber is visible at once, C = 250 microns may be quite acceptable, thus giving Δs = 5 mm. Measuring at high magnification, C = 5 microns may already be noticeable, giving Δs = 100 microns. It thus seems possible to see a large fraction of the chamber at low magnification, and, at high magnification, to get good resolution in "Z".

At this time there has been little experience in the analysis of holograms. However, with the current interest in Europe and here, it is expected that the learning curve will be very steep. We describe here a simple and cheap device that is useful for gaining experience and which has actually been constructed

at Rutherford Laboratory[61] by making small modifications to a Vanguard measuring machine (see Fig. 7). The ordinary Vanguard light source is replaced by a laser, spatial filter, and beam expander. The film platen is mounted on a stage with 50 mm of vertical travel (this will have to be digitized). Two TV cameras are than arranged to view the holographic image at magnifications of 22X and 200X as seen on TV monitors which replace the viewing screen.

This device, which is adequate for the accurate measurement of holograms was described by Colin Fisher at a conference[61] at Rutherford on January 19/20, 1981 as costing about $7,000 and "about $25,000 to do right". This does not, of course, include the cost of the Vanguard.

Tests are now being carried out both of the taking and of the reprojection of holograms to gain a better and more detailed understanding. Finally we note that the scanning of these holograms can be significantly speeded up by using off-line analysis of the donwstream detectors to predict the position of the vertex.

VII. Cost Estimate

To provide the cost scale for this proposed experiment, we have made a "first pass" estimate of the cost of the apparatus as presented in this proposal. As discussed in the Introduction, we are in the process of making a more complete design, but the following estimates are expected to be representative of the needs of this experiment:

Cost Summary for HQS

a)	Vertex Magnet		$1,187 K	(1)
b)	$\check{C}_1$		122 K	
c)	$\check{C}_2$		122 K	
d)	PWC System (P_1-P_{12})		1,680 K	
e)	Muon Steel Absorber (2x1.6x7.3m^3)		400 K	(2)
f)	On-Line Computer		200 K	
g)	Hodoscope Systems (H_a,H_b,H_1-H_3)		158 K	
h)	Trigger Processor		250 K	
i)	Shower Detector		650 K	
j)	Microsonic Detector (MSD)	i) R + D	100 K	
		ii) chamber	200 K	
k)	High Resolution Streamer Chamber (HRSC)			
		i) R + D	250 K	
		ii) chamber	250 K	
		TOTAL	$5,569 K	

(1) This magnet is the size and has the field of a magnet which has already been built at Fermilab (MPS).

(2) This is the cost of new steel. We may be able to use some steel that currently exists at Fermilab.

References

1. M. Glück et al Phys Rev D17, 2324 (1978).
2. V.G. Kartvelishvili et al, Phys. Lett. 78B, 615 (1978); A. Ali et al, Phys. Lett. 83B, 375 (1979).
3. S. Wojcicki, SLAC-PUB-2603, XXth Int. Conf. on HEP, Madison, Wisc. (1980).
4. M. Perl, Ann. Rev. Nucl. Part. Sci. 30, 299 (1980).
5. C. Quigg and J.L. Rosner, Phys. Rev. D19, 1532 (1979).
6. V. Barger, T. Gottschalk and R.J.N. Phillips, Phys. Lett. 82B, 445 (1979).
7. A. Ali, Zeit, F. Physik, C1, 25 (1979).
8. G.C. Branco and H.P. Nilles, Nucl. Phys. B151, 529 (1979).
9. M.S. Chanowitz, Int. Symposium on High Energy e^+e^- Interactions, Vanderbilt (1980).
10. G.L. Kane and S. Raby, Phys. Lett. 89B, 203 (1980).
11. S.S. Gerstein and M.Y. Khlopov IHEP 76-73 (1976); V.A. Novikov et al, Phys. Rev. Lett. 38, 626, 791 (E) (1977); R.N. Cahn and S.D. Ellis, U. Mich report UM-HE 76-45 (1976).
12. E. Golowich, Phys. Lett. 91B, 271 (1980).
13. B. Guberina et al, Phys. Lett 90B, 169 (1980).
14. G.L. Kane and R. Thun, Phys. Lett. 94B, 513 (1980).
15. J.S. Hagelin, Phys. Rev. D20, 2893 (1979).
16. V. Barger, W.F. Long, and S. Pakvasa, Phys. Rev. D21, 174 (1980).
17. E. Ma, W.A. Simmons and S.F. Tuan, Phys. Rev. D20, 2888 (1979).
18. V. Barger and S. Pakvasa, Phys. Rev. Lett 43, 812 (1979).
19. M. Bander, D. Silverman and A. Soni, Phys.Rev. Lett. 43, 242 (1979).
20. A.B. Carter and A.I. Sanda, Phys. Rev. Lett. 45, 952 (1980).
21. M.B. Wise, SLAC-PUB-2574, XXth Int. Conf. HEP, Madison (1980).
22. Y. Fujimoto, Lett. Nuovo Cimento 29, 283 (1980).
23. E.H. Thorndike, XXth Int. Conf. on HEP, Madison, UR-758 (1980).
24. S.L. Glashow, Phys. Rev. Lett. 45, 1914 (1980); H. Georgi and S.L. Glashow, Nucl. Phys. B167, 173 (1980).

25. V. Barger and S. Pakvasa, Phys. Lett. 81B, 195 (1979).

26. S. Pakvasa, UH-511-410-80, XXth Int. Conf. HEP, Madison (1980).

27. C. Bebek et al, Phys. Rev. Lett. 46, 84 (1981); K. Chadwick et al, PRL 46, 88 (1980).

28. B. Alper et al, Nucl. Phys. B100, 237 (1975).

29. A. Diamant-Berger et al, Phys. Rev. Lett. 43, 1774 (1979).

30. W. Bacino et al, Phys. Rev. Lett. 42, 749 (1979); Particle Data Group, Rev. Mod. Phys. 52 April (1980).

31. A. Diamant-Berger et al, Phys. Rev. Lett. 44, 507 (1980).

32. Progress Report on Results from the CLEO Detector, Int. Conf. on HEP, Madison, CLNS-80/464 (1980).

33. M. Kobayashi and K. Maskawa, Progr. Theor. Phys. 49, 652 (1973).

34. R.E. Shrock and L.L. Wang, Phys. Rev. Lett. 41, 1692 (1978).

35. R.E. Shrock, S.B. Treiman and L.L. Wang, Phys. Rev. Lett. 42, 1589 (1979); V. Barger et al, Phys. Rev. Lett. 42, 1585 (1979).

36. V. Barger et al, Int. Conf. HEP, Madison, SLAC-PUB-2596 (1980)

37. J. Ellis et al, Nucl. Phys. B131, 285 (1977).

38. M. Kuroda, Bielefeld Preprint BI-TP 80/14 (1980).

39. D. Scharre, Proc. Int. Symp. on High Energy e^+e^- Interactions, Vanderbilt (1980).

40. J.H. Kühn et al, Z.F. Physik, C5, 117 (1980).

41. M.B. Wise, Phys. Lett. 89B, 229 (1980).

42. T.A. DeGrand and D. Toussaint, Phys. Lett. 89B, 256 (1980).

43. H. Fritzsch, Phys. Lett. 86B, 164, 343 (1979); 90B, 167 (1980).

44. T.G. Rizzo Phys. Rev. D20, 706 (1979); Phys. Rev. D18, 1569 (1978).

45. N. Cabibbo and L. Maiani, Phys. Lett. 87B, 366 (1979).

46. V. Blobel et al, Phys. Lett. 59B, 88 (1975); B.Y. Oh and G.A. Smith, Nucl. Phys. B49, 13 (1972); J.W. Waters et al, Nucl. Phys. B17, 445 (1970).

47. K.J. Anderson et al, Phys. Rev. Lett. 37, 799 (1976); D. Brick et al, Phys. Rev. D20, 2123 (1979).

48. P.L. Woodworth et al, Phys. Lett. 65B, 89 (1976).

49. Tu Tung-Sheng, Phys. Lett. 89B, 237 (1980).

50. G. Matthiae, CERN-EP/80-183 (1980), to be publ. in Rivista del Nuovo Cimento.

51. R. Barate et al, and Y. Lemoigne, papers submitted to 1979 Int. Conf. on Photon and Lepton Interactions, Batavia, (1979).

52. WA 11 Status Report, Private Communication from M. Abolins (1979).

53. R.N. Coleman et al, Phys. Rev. Lett. 44, 1313 (1980).

54. P.J. Carlson and R. Kiesler, N.I.M. 161, 421 (1979).

55. D. Müller, Phys. Rev. D5, 2677 (1972).

56. S.L. Stone et al, Nucl. Instr. and Methods, 151, 387 (1978).

57. M. Basile et al, Nucl. Instr. and Methods 163, 93 (1979); D.P. Barber et al, Phys. Reports 63, 337 (1980); C. Ankenbrandt et al, Fermilab Internal Report, Unpublished (1979).

58. "A Modular Trigger Processing System for High Energy Physics Experiments", E. Barsotti et al, Fermilab TM-823; "ECL/CAMAC Trigger Processor Documentation", E. Barsotti et al, Fermilab TM-821 (1978).

59. Y. Afek, C. Leroy, and B. Margolis, Phys. Rev. D23, 760 (1981).

60. Proceedings of the 1979 International Symposium on Lepton and Photon Interactions at High Energies, August 23-29, (1979), Fermi National Accelerator Laboratory, P. 559.

61. Conference on Holographic Techniques for Bubble Chamber Physics, Rutherford Laboratory, January 19/20, 1981.

Figure Captions

Figure 1 Feynman diagrams for (a) - (d) production of b quarks; production of ψ/T through (e) fusion of q=u,d,s quarks, and (f) fusion of c,b quarks.

Figure 2 Layout of proposed experiment - heavy quark spectrometer.

Figure 3 Momentum spectrum for $K^{\pm}$ produced by $B \to D\mu\nu 4\pi$ and $B \to D7\pi$ followed by $D \to K^{\pm}\mu\nu$.

Figure 4 Single muon acceptance times branching ratio as a function of the minimum cutoff applied to the transverse momentum of the muon.

Figure 5 Trigger rate per NN interaction as a function of the minimum cutoff applied to the transverse momentum of the muon for muons from $\pi^{\pm}$, $K^{\pm}$, $D\bar{D}$ and $B\bar{B}$ decays. The dotted line shows the trigger rate for $B \to D\mu\nu$. The dashed line shows the trigger rate for $B \to D\mu\nu 4\pi$.

Figure 6 The relation between lifetime sensitivity and bubble diameter in LEBC.

Figure 7 Rutherford Laboratory design of a Vanguard Optical Layout for Holography.

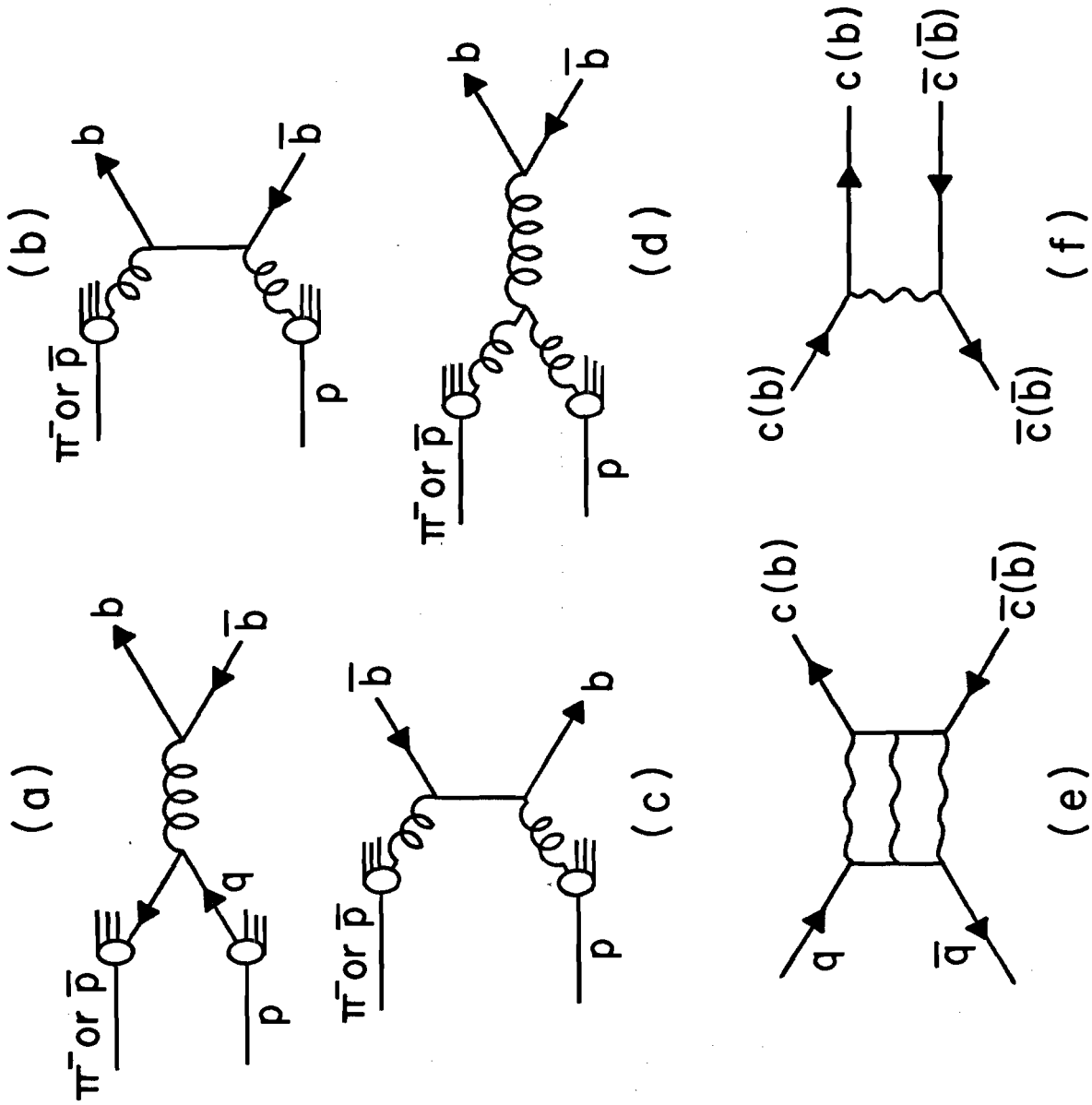

Figure 1

HEAVY QUARK SPECTROMETER

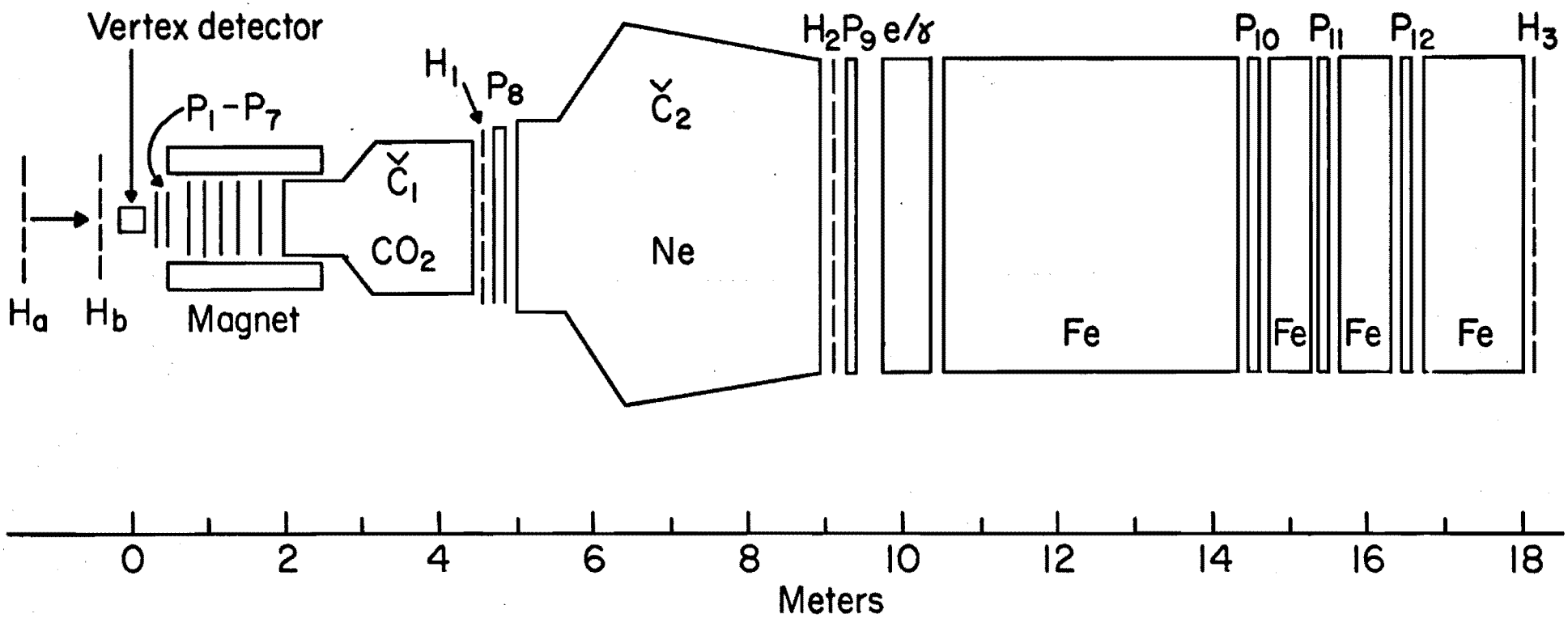

Figure 2

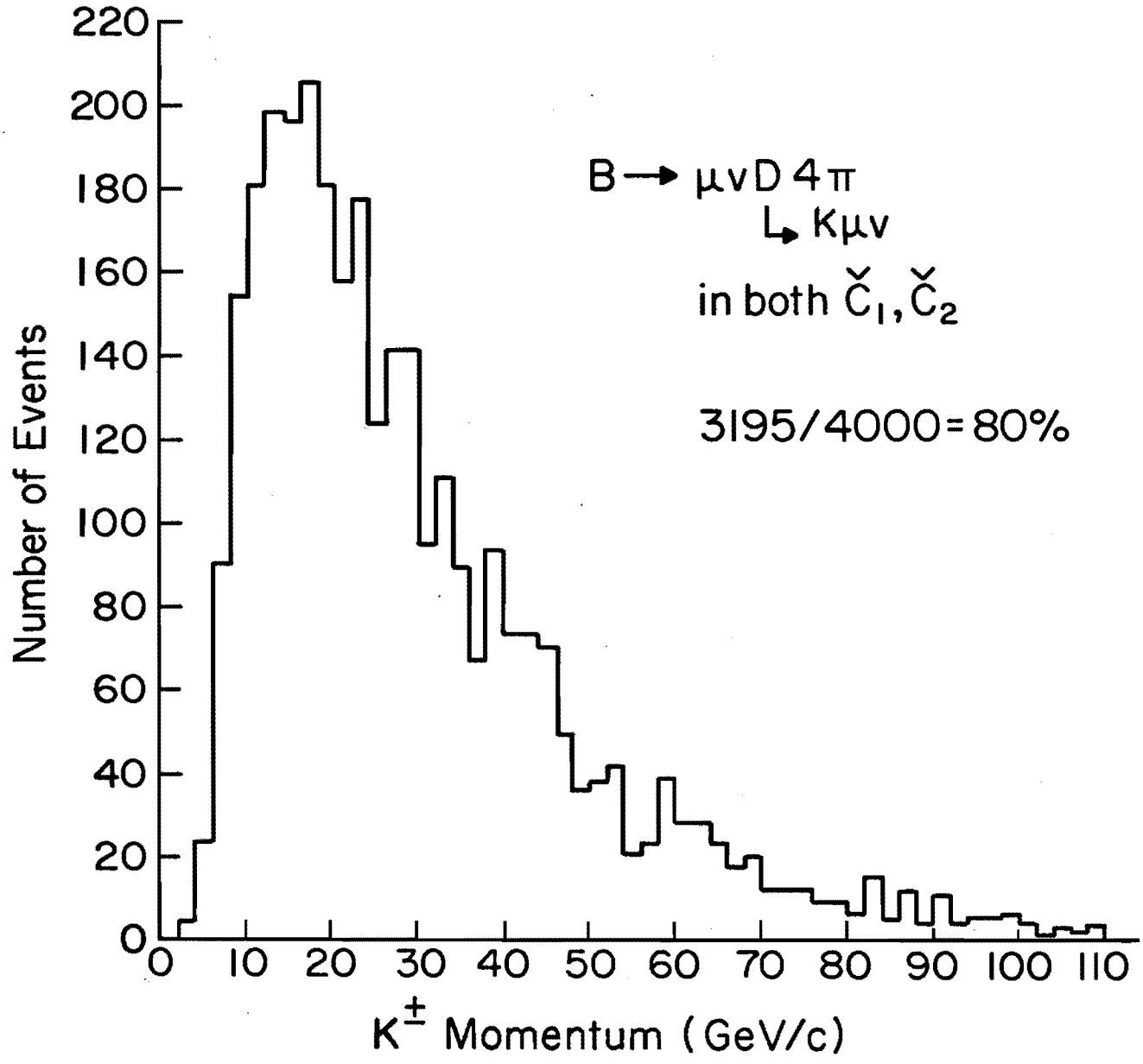
220
200
180
160
140
120
100
80
60
40
20
0
Number of Events
0 10 20 30 40 50 60 70 80 90 100 110
K± Momentum (GeV/c)
B → μνD 4π
↳ Kμν
in both Č1, Č2
3195/4000 = 80%

Figure 3

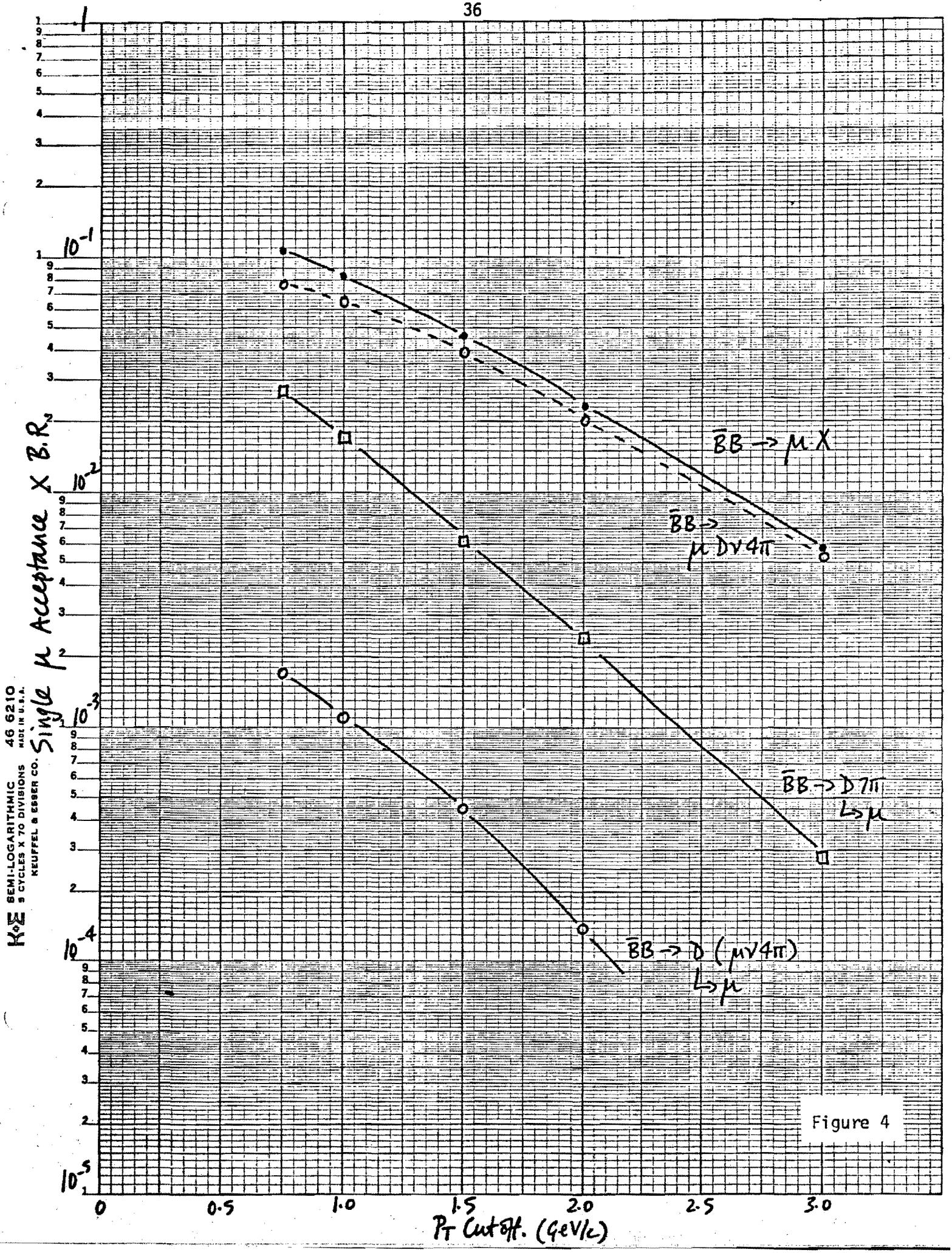
Single μ Acceptance X B.R.
10^{-1}
10^{-2}
10^{-3}
10^{-4}
10^{-5}
$\bar{B}B \to \mu X$
$\bar{B}B \to \mu D\nu 4\pi$
$\bar{B}B \to D\,7\pi$
$\hookrightarrow \mu$
$\bar{B}B \to D\,(\mu\nu 4\pi)$
$\hookrightarrow \mu$
0
0.5
1.0
1.5
2.0
2.5
3.0
P_T Cutoff. (GeV/c)
K+E SEMI-LOGARITHMIC 46 6210
5 CYCLES X 70 DIVISIONS MADE IN U.S.A.
KEUFFEL & ESSER CO.

Figure 4

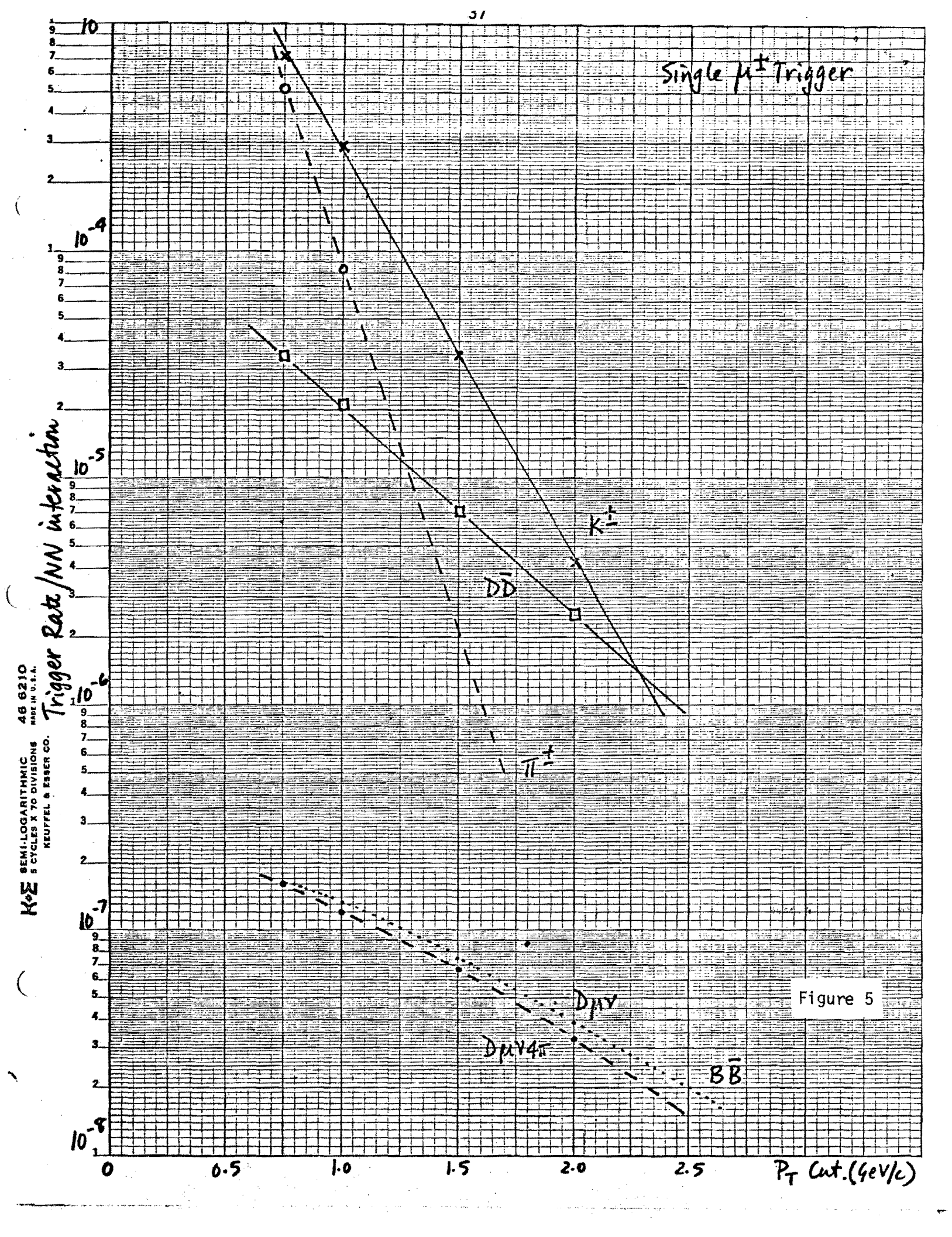
Single $\mu^{\pm}$ Trigger
Trigger Rate/NN interaction
$K^{\pm}$
$D\bar{D}$
$\pi^{\pm}$
$D\mu\nu$
$D\mu\nu 4\pi$
$B\bar{B}$
10^{-4}
10^{-5}
10^{-6}
10^{-7}
10^{-8}
0
0.5
1.0
1.5
2.0
2.5
P_T Cut. (GeV/c)
K&E SEMI-LOGARITHMIC 5 CYCLES X 70 DIVISIONS KEUFFEL & ESSER CO. 46 6210 MADE IN U.S.A.

Figure 5

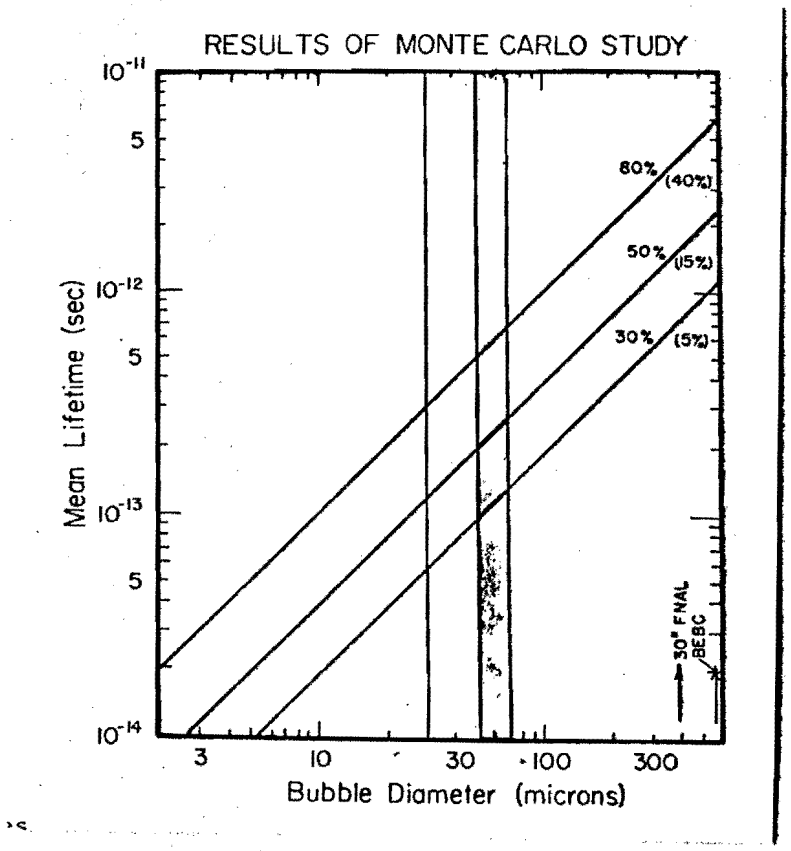

Figure 6

Results of the Monte Carlo calculation carried out for charmed particle detection in a visual detector by the Rutherford group for the LEBC collaboration.[60] The diagonal lines give the relationship between charmed particle lifetime and bubble diameter (equivalent to track width for the HRSC) for various detection efficiencies.

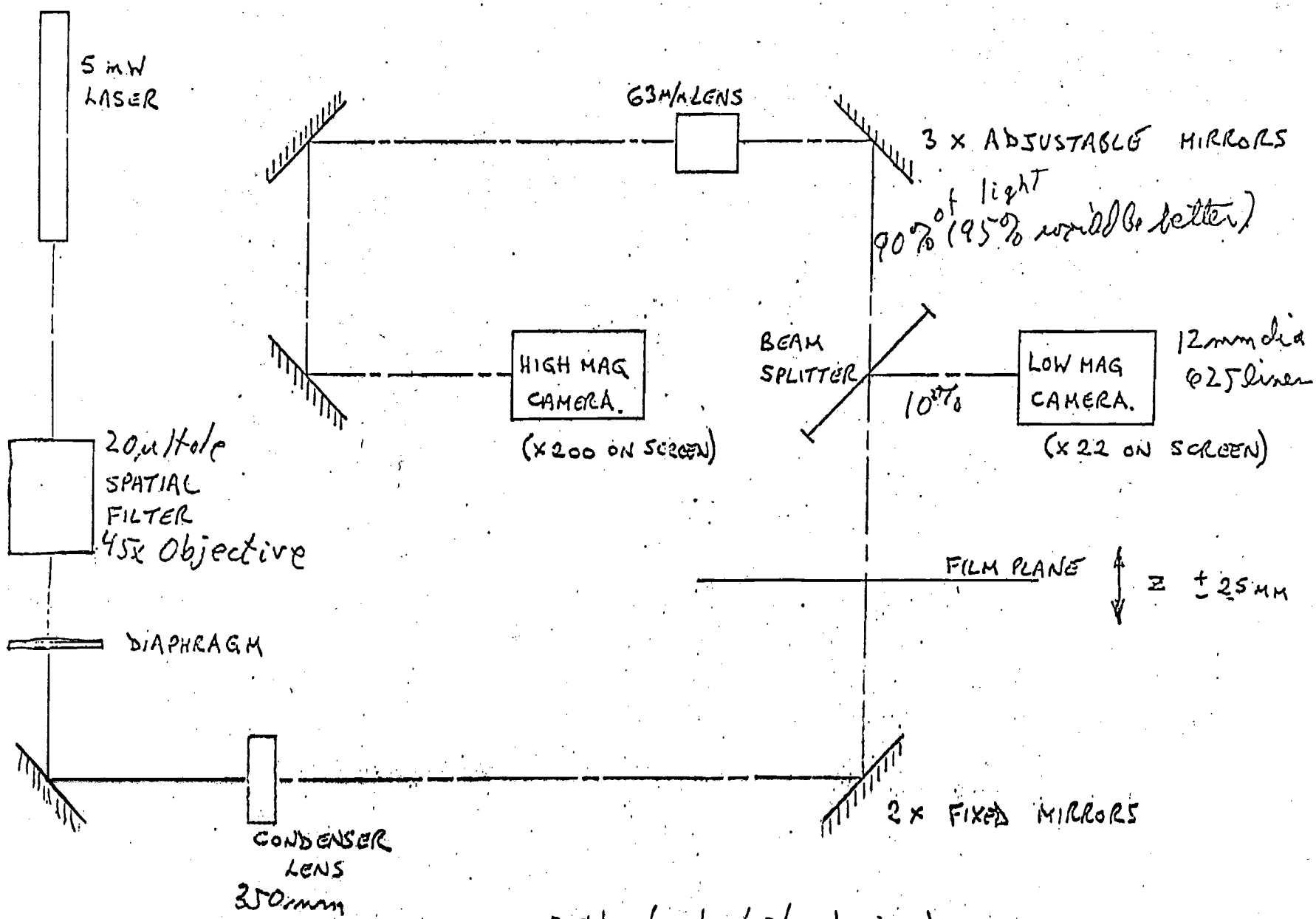

(Rutherford Lab design)

VANGUARD OPTICAL LAYOUT FOR HOLOGRAPHY

Figure 7

APPENDIX I

Theoretical Estimates of B-Meson Decay Rates

The ground state mesons ($b\bar{u}$, $b\bar{d}$, $b\bar{s}$, $b\bar{c}$) can only decay weakly. Furthermore, since the dominant transition $b \to t$ is forbidden kinematically, all decays of the B-mesons are Cabibbo suppressed. To calculate the various decay rates for heavy quarks, the standard SU(2)XU(1) six-quark model of Kobayashi and Maskawa[33] is commonly used with the three left-handed doublets of leptons and quarks,

$$\binom{\nu_e}{e}, \binom{\nu_\mu}{\mu}, \binom{\nu_\tau}{\tau} \quad \text{and} \quad \binom{u}{d'}, \binom{c}{s'}, \binom{t}{b'}.$$

The standard flavor-basis mass eigenstates d, s, and b (each with charge -1/3) are related to the gauge-group quark eigenstates d', s' and b' by a 3X3 unitary transformation U:

$$\begin{pmatrix} d' \\ s' \\ b' \end{pmatrix} = U \begin{pmatrix} d \\ s \\ b \end{pmatrix} = \begin{pmatrix} c_1 & s_1c_3 & s_1s_3 \\ -s_1 c_2 & c_1c_2c_3 - s_2s_3e^{i\delta} & c_1c_2s_3 + s_2c_3e^{i\delta} \\ s_1 s_2 & c_1s_2c_3 + c_2s_3e^{i\delta} & c_1s_2s_3 - c_2c_3e^{i\delta} \end{pmatrix} \begin{pmatrix} d \\ s \\ b \end{pmatrix}, \qquad \text{(AI-1)}$$

Various authors have put limits on the values of θ_i and δ. In general, there is the usual quadrant ambiguity for δ: $\xi = \text{sign}(c_\delta) = \pm 1$. Some recent estimates[34,35] are shown below for $\xi = \pm 1$, $m_t = 15$, 30 GeV:

Case	ξ	m_t	$\lvert S_1 \rvert$	$\lvert S_2 \rvert$	$\lvert S_3 \rvert$	$\lvert S_\delta \rvert$
(a)	+1	15 GeV	0.228	0.20	0.278	1.1×10^{-2}
(b)	-1	15 GeV		0.50		0.5×10^{-2}
(c)	+1	30 GeV		0.10		1.0×10^{-2}
(d)	-1	30 GeV		0.40		0.3×10^{-2}

(AI-2)

Using the values in (AI-2), we can solve for the elements of U (where we follow Ref. 35 with $0 < \theta_1, \theta_2, \theta_3 < 90°$ and $m_t = 15$ GeV):

	(a) $0 < \delta < 90°$	(b) $90° < \delta < 180°$
$U_{11} = c_1$	0.974	0.974
$U_{12} = s_1c_3$	0.219	0.219
$U_{13} = s_1s_3$	0.063	0.063
$U_{21} = -s_1c_2$	-0.223	-0.197
$U_{22} = c_1c_2c_3 - s_2s_3e^{i\delta}$	$0.861 - 0.61 \times 10^{-3}i$	$0.950 - 7.0 \times 10^{-3}i$
$U_{23} = c_1c_2s_3 + s_2c_3e^{i\delta}$	$0.457 + 2.1 \times 10^{-3}i$	$-0.247 + 2.4 \times 10^{-3}i$
$U_{31} = -s_1s_2$	-0.046	-0.114
$U_{32} = c_1s_2c_3 + c_2s_3e^{i\delta}$	$0.459 + 3.0 \times 10^{-3}i$	$0.227 + 1.2 \times 10^{-3}i$
$U_{33} = c_1s_2s_3 - c_2c_3e^{i\delta}$	$-0.888 - 1.0 \times 10^{-2}i$	$0.967 - 4.2 \times 10^{-3}i$

In the KM model, the $\Delta B = \pm 1$ (flavor-changing) charged weak current can be written as

$$J_\mu^{\Delta B = 1,C} = (\bar{u}\ \bar{c}\ \bar{t})\ \gamma_\mu\ (1 - \gamma_5)\ U \begin{pmatrix} d \\ s \\ b \end{pmatrix},$$

and the bottom-flavor-changing neutral current as

$$J_\mu^{\Delta B=1,\ N} = (\bar{d}\ \bar{s}\ \bar{b})\ \gamma_\mu\ (1 - \gamma_5)\ U \begin{pmatrix} d \\ s \\ b \end{pmatrix}.$$

The total weak $\Delta B = 1$ effective Hamiltonian is

$$H^{\Delta B=1} = H_C^{\Delta B=1} + H_N^{\Delta B=1},$$

where

$$H_{C(N)}^{\Delta B=1} = \frac{G_F}{\sqrt{2}}\ J_\mu^{\Delta B=1,C(N)}\ J^\mu_{\Delta B=1,C(N)} + \text{h.c.}$$

The $J_\mu^{\Delta B=0,C(N)}$ would be the charged (neutral) currents already measured in the decays of bottomless particles.

To investigate explicitly the dominant hadronic decays of the b quark as a function of m_t, ξ:

$$H = (U_{13}^+ \bar{b}u + U_{23}^+ \bar{b}c)\ (U_{11}\bar{u}d + U_{12}\bar{u}s + U_{21}\bar{c}d + U_{22}\bar{c}s)$$

$$= U_{13}^+ U_{11} b\bar{u}\bar{u}d + \ldots .$$

Hence we can calculate $|U_{ij}U_{kn}|^2$ for each transition:

	(a) m_t=15	(b)	(c) m_t=30	(d)
$b\to u\bar{u}d$	0.0038	0.0038	0.0038	0.0038
$b\to u\bar{u}s$	0.0002	0.0002	0.0002	0.0002
$b\to u\bar{c}d$	0.0002	0.0002	0.0002	0.0002
$b\to u\bar{c}s$	0.0029	0.0036	0.0032	0.0037
$b\to c\bar{u}d$	0.1981	0.0579	0.1264	0.0175
$b\to c\bar{u}s$	0.0100	0.0029	0.0064	0.0009
$b\to c\bar{c}d$	0.0104	0.0024	0.0069	0.0008
$b\to c\bar{c}s$	0.1548	0.0551	0.1086	0.0174

(AI-3)

Thus we see that the dominant decays are $b\to c\bar{u}d$ and $b\to c\bar{c}s$.

Using these expressions, Barger et al [36] have investigated the role of "nonspectator" diagrams in B decays. The net spectator contribution including strong enhancement factors is:

$$\Gamma_{spect.}(B) = \gamma_B[7.59\ |U_{bu}|^2 + 3.07|U_{bc}|^2],$$

where $\gamma_B = G_F^2 m_b^5/192\pi^3 = 6 \times 10^{13} s^{-1}$.

After including both spectator and nonspectator contributions, they find:

$$\begin{aligned}
\Gamma(B_d^\circ) &= \gamma_B[10.41|U_{bu}|^2 + 4.95\ |U_{bc}|^2] \\
\Gamma(B_s^\circ) &= \gamma_B[\ 8.67|U_{bu}|^2 + 3.75\ |U_{bc}|^2] \\
\Gamma(B_u^-) &= \gamma_B[\ 9.67|U_{bu}|^2 + 3.07\ |U_{bc}|^2] \\
\Gamma(B_c^-) &= \gamma_B[\ 7.69|U_{bu}|^2 + 5.17\ |U_{bc}|^2]
\end{aligned} \qquad \text{(AI-4)}$$

Thus these rates are not dramatically different from the spectator rate.[36]

B-Meson Lifetimes and Branching Ratios

Given these decay rates we can calculate the total decay rate and hence the lifetime and branching ratios for various decay modes.

(i) B-Meson Lifetimes

From the values given above, we find $\tau_{B^\circ} = (0.3 - 2) \times 10^{-13}$ sec. We might expect that τ_{B^-} is a little larger since some of the diagrams for B_u^- decay cannot occur [$\Gamma(B^-_u) < \Gamma(B^\circ_d)$]. However, from Eq. (AI-4) we see that the ratio of $\tau_{B^-}/\tau_{B^\circ}$ should be $\sim$ 1.1 - 1.6 rather than $\sim$ 3-4 as is found for $\tau_{D^+}/\tau_{D^\circ}$.

(ii) Leptonic Decays

The decay rate for $B^- \to \tau^-\nu_\tau$ is (for m_τ = 1784 MeV):

$$\Gamma(B^- \to \tau^-\nu_\tau) = |U_{13}|^2\ (1-m_c^2/m_b^2\ )^2 m_\tau^2 \cdot G_F^2 f_B^2 m_b/8\pi$$

and hence [37] [the μ and e leptonic decays are down by $(m_\mu/m_\tau)^2$ etc.]:

$$\begin{aligned}
B(B^- \to \tau^-\nu_\tau) &= 0.19\ |U_{13}|^2/|U_{23}|^2 \\
&= 3.6 \times 10^{-3} \text{ and } 12.4 \times 10^{-3} \text{ for } m_t = 15 \text{ GeV} \\
&= 5.7 \times 10^{-3} \text{ and } 40.9 \times 10^{-3} \text{ for } m_t = 30 \text{ GeV}.
\end{aligned}$$

Note that the observation of this decay mode would provide a measurement of the weak decay constant, f_B.

(iii) Semileptonic Decays

The semileptonic decays can be calculated in the same way as above. The τ^- semileptonic channel is suppressed by phase space. Barger et al [36] find the semileptonic branching ratios to be

$$B_{e+\mu}(B_d) = \gamma_B[2.11\ |U_{bu}|^2 + 0.92\ |U_{bc}|^2]/\Gamma(B_d)$$

$$B_{e+\mu}(B_u) = \gamma_B[2.25\ |U_{bu}|^2 + 0.92\ |U_{bc}|^2]/\Gamma(B_u)$$

Again we see that the charmed final states should dominate. From these equations, Barger et al calculate that

$$B_{e+\mu}(B_d^\circ) = 2 \times 10\%$$

$$B_{e+\mu}(B_u^-) = 2 \times (12\text{-}15)\%$$

Other recent calculations [38] also based on soft gluon interaction effects inside hadrons have been performed for both D and B decays:

$$B(D^\circ \to e\nu X) = 4.8\% \quad (\text{Data}^{(39)}: < 4\% \text{ or } 6\pm5\%)$$

$$B(D^+ \to e\nu X) = 26\% \quad (\text{Data}^{(39)}: \ 23\pm6\% \text{ or } 17\pm6\%)$$

and $B(B^\circ \to e\nu X) \simeq 9\%,$

$$B(B^- \to e\nu X) \simeq 16\%,$$

in good agreement with recent results from CESR[27] of $13 \pm 3(\pm3)\%$.

(iv) Nonleptonic:

Because of the heavy mass of the b quark, we expect the B Meson to decay into many particles and to have many hadronic decay modes. The dominant modes involve charm and some of the more interesting modes involve $B_q \to (c\bar{q})(\bar{c}s)$. Measurement of the inclusive rate for $B \to \psi X$ will yield information about the dynamics of nonleptonic decays. As we have seen, the lowest order effective Hamiltonian is

$$H_{eff} \propto (\bar{b}c)(\bar{c}s) \propto C(\bar{b}_\alpha s_\beta)(\bar{c}_\beta c_\alpha)$$

where the second line is obtained by Fierz rearrangement, the color indices are summed over, and $C = 1/3$ for a bare Hamiltonian and $C=1/3(2f_+ - f_-)$ for an effective Hamiltonian. Thus measurement of the inclusive rate gives information about the importance of color rearrangement due to gluonic final state interactions. $\bar{c}_\beta c_\alpha$ is in a color singlet for 1/9 of the final

states and in a color octet for 8/9. Therefore there is a factor of 9 difference in the predicted rate for $B \to \psi X$ depending on whether or not we neglect color rearrangement. (The color octet can emit soft gluons to become a singlet.)

Using $BR(B \to \psi X) \sim BR(b \to c\bar{c}s)\ BR(c\bar{c} \to \psi)$, this type of decay has been estimated by many authors. The most extensive calculations have been made by Kühn et al [40]. Their results for the branching ratios for B into charmonium states are shown below in terms of C^2(for m_B=5 GeV).

$(c\bar{c})$	$B(B \to (c\bar{c})X)$	Kühn et al Ref. 40 C=1/3	Wise Ref.41	DeGrand et al Ref.42	Fritzch Ref. 43
$\eta_c(3.0)$	$0.12C^2$	1.3%		∿ 1%	
J/ψ (3.095)	$0.21C^2$	2.3%	∿ 2%	∿ 1.8%	∿3%
P_c/χ_1 (3.51)	$0.07C^2$	0.8%			
ψ' (3.686)	$0.07C^2$	0.8%	0.6%	∿ 0.4%	
ψ'' (3.771)	$0.01C^2$	0.1%			
4.04	$0.02C^2$	0.2%			
4.16	$0.02C^2$	0.2%			
4.41	$0.003C^2$	0.03%			
Inclusive $\sum_i (c\bar{c}_i)+s$	$0.58C^2$	6.4%			

Finally, we consider strange particle production in B decays.

A detailed calculation using nonleptonic enhancement factors yields [36]

$$\langle n_K(B_d) \rangle > \gamma_B[1.9\ |U_{bu}|^2 + 5.7\ |U_{bc}|^2]/\Gamma(B_d)$$

$$\langle n_K(B_u) \rangle > \gamma_B[4.3\ |U_{bu}|^2 + 3.8\ |U_{bc}|^2]/\Gamma(B_u)$$

with an additional 15-20% from $s\bar{s}$ pair creation from the vacuum. This result yields:

$b \to c$ $\quad \langle n_K(B_d) \rangle \simeq 1.4$; $\quad \langle n_K(B_u) \rangle \simeq 1.5$

$b \to u$ $\quad \simeq 0.2$ $\quad \simeq 0.5$.

For comparison with experiment, CLEO has studied strange particle production at the $\Upsilon(4S)$. They find [23,32]

$$\langle n_K \rangle = 2.5 \pm 0.5 \pm 0.6$$

This is $\sim 2\sigma$ more than the calculations above estimated and would imply that

$$(b \to cW^-) >> (b \to uW^-)$$

as the calculations based on the weak mixing angles suggest.

APPENDIX II

Estimates of Rates for Lepton Final States

To find the possible multilepton final states possible from b decay, it is instructive [5,8,44,45] to consider the following table [5] for the process

$$b(-1/3) \rightarrow \text{quark}(+2/3) + W^-$$

$W^- \rightarrow$	$e^-\bar{\nu}_e$	$\mu^-\bar{\nu}_\mu$	$\tau^-\bar{\nu}_\tau$			$\bar{u}$ (d,s)	$\bar{c}$ (d,s)		
			e^-	μ^-	NL		e^-	μ^-	NL
quark ↓									
u or c→NL	e^-	μ^-	e^-	μ^-	-	-	e^-	μ^-	-
$c \rightarrow e^+$	e^+e^-	$e^+\mu^-$	e^+e^-	$e^+\mu^-$	e^+	e^+	e^+e^-	$e^+\mu^-$	e^+
$c \rightarrow \mu^+$	μ^+e^-	$\mu^+\mu^-$	μ^+e^-	$\mu^+\mu^-$	μ^+	μ^+	μ^+e^-	$\mu^+\mu^-$	μ^+

Now we can write down the sources of single μ^- or μ^+, and opposite sign $\mu^+\mu^-$. The Same rates apply to single e^- or e^+ or μ^-e^+ or μ^+e^- if we let $B(\tau \rightarrow e) = B(\tau \rightarrow \mu)$.

a) From single b decay:

single $\mu^-(e^-)$

i) $b \rightarrow \mu^-\bar{\nu}_\mu X$ $\quad (b \rightarrow c\mu^-)(c \rightarrow X) + (b \rightarrow u\mu^-) + (b \rightarrow u\bar{c}X)(\bar{c} \rightarrow \mu^-)$

ii) $b \rightarrow c\bar{c}X$, $c \rightarrow \mu^-\bar{\nu}_\mu X$ $\quad (b \rightarrow c\bar{c}X)(c \rightarrow X)(\bar{c} \rightarrow \mu^- X)$

iii) $b \rightarrow \tau^-\bar{\nu}_\tau X$, $\tau \rightarrow \mu^-\bar{\nu}_\mu\nu_\tau$ $\quad (\tau \rightarrow \mu X)[(b \rightarrow c\tau^-)(c \rightarrow X) + (b \rightarrow u\tau)]$

single $\mu^+(e^+)$

i) $b \rightarrow cX$, $c \rightarrow \mu^+\nu_\mu X$ $\quad (c \rightarrow \mu X)[(b \rightarrow c\bar{u}) + (b \rightarrow \bar{c}c)(c \rightarrow X) + (c \rightarrow \tau)(\tau \rightarrow X)]$

opp. sign $\mu^+\mu^-$

i) $b \rightarrow c\mu^-\nu_\mu X$, $c \rightarrow \mu^+\nu_\mu X$ $\quad (b \rightarrow c\mu^-)(c \rightarrow \mu X)$

ii) $b \rightarrow c\bar{c}X$, $c \rightarrow \mu^-\bar{\nu}_\mu X$, $\bar{c} \rightarrow \mu^+\nu_\mu X$ $\quad (b \rightarrow c\bar{c}X)(c \rightarrow \mu)^2$

iii) $b \to c\tau^- \bar{\nu}_\tau X$ $\qquad (b \to c\tau)(c \to \mu)(\tau \to \mu)$

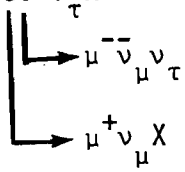

Evaluating these we find:

$B(\mu^-)$: $B(\mu^+)$: $B(\mu^+\mu^-)$: $B(\text{no } \mu^\pm) = 0.13: 0.05: 0.01: 0.81$

(b) from double b decay:

opposite sign $\mu^+\mu^-$	i)	$(b \to \mu^+\mu^- X)(\bar{b} \to X) + (b \to X)(\bar{b} \to \mu^+\mu^- X)$
	ii)	$(b \to \mu^- X)(\bar{b} \to \mu^+ X)$
	iii)	$(b \to \mu^+ X)(b \to \mu^- X)$
Like sign $\mu^+\mu^+$ (or $\mu^-\mu^-$)	i)	$(b \to \mu^+ X)(\bar{b} \to \mu^+ X)$
Tri-leptons $\mu^+\mu^-\mu^+$ (or $\mu^-\mu^+\mu^-$)	i)	$(b \to \mu^+ X)(\bar{b} \to \mu^-\mu^+ X)$
	ii)	$(b \to \mu^+\mu^- X)(\bar{b} \to \mu^+ X)$
Tetra-Leptons $2\mu^+2\mu^-$	i)	$(b \to \mu^+\mu^- X)(\bar{b} \to \mu^+\mu^- X)$

These branching ratios are:

$B(\mu^+\mu^-)$: $B(\mu^+\mu^+)$: $B(3\mu)$: $B(4\mu) = 0.038: 0.008: 0.002: 1.2 \times 10^{-4}$

Finally, we can calculate the branching ratios for this theory for different lepton triggers.

1.	$\geq 1\mu^+$ (or μ^-, $e^\pm$)	0.199×2	$= 0.40$
2.	$\geq 2\mu^+$ (or $2\mu^-$, $2e^\pm$, $\mu^\pm e^\pm$)	$0.038 + 0.0021 + 1.2 \times 10^{-4}$	$= 0.040$
3.	$\geq 3\mu$ (or $2\mu e$, $3e$)	$0.0021 + 1.2 \times 10^{-4}$	$= 0.0022$
4.	$2\mu^+2\mu^-$ (or $4e$, $2\mu 2e$)	$(1.23 \times 10^{-4})^2$	$= 1.5 \times 10^{-8}$
5.	$B \to \psi \to 2\mu$ (or $\psi \to 2e$)	$(0.02 \times 0.07) \times 2$	$= 0.0028$
6.	$B \to \tau^- \to \mu^-$ (or $\tau^- \to e^-$)	0.06×0.171	$= 0.010$

APPENDIX III

Estimates of Hadronic Production Cross Sections of B-Mesons

Current folklore would suggest that unbound heavy quarks (c,b,t...) should be produced at least as copiously as bound ($q\bar{q}$) states (ψ, T...). Such phenomenological estimates have some experimental basis for strange and charm quarks:

a) for pp at 24 GeV/c [46], $\frac{\sigma(K\bar{K}X)}{\sigma(\phi X)} = \frac{2.5\ \text{mb}}{158 \pm 35\mu\text{b}} = 15.8$

for pp at 150 GeV/c [47], $\frac{\sigma(K\bar{K}X)}{\sigma(\phi X)} = \frac{13.4\ \text{mb}}{660 \pm 200\ \mu\text{b}} = 20.3 \pm 6$

for exclusive channels in π^-p at 19 GeV/c [48],

$$\frac{\sigma(K\bar{K}\ 3\pi p)}{\sigma(\phi 3\pi p)} = 119.3 \pm 30$$

b) For ψ and $D\bar{D}$ production we find for

πN at 150 GeV/c, $\frac{\sigma(D\bar{D}X)}{\sigma(\psi X)} = \frac{15\text{-}20\mu\text{b}}{94 \pm 31\text{nb}} = 150\text{-}200$

pN at 400 GeV/c, $\frac{\sigma(D\bar{D}X)}{\sigma(\psi X)} = \frac{25\mu\text{b}}{243\text{nb}} = 103$

and

πN at 400 GeV/c, $\frac{\sigma(D\bar{D}X)}{\sigma(\psi X)} = \frac{30\text{-}40\mu\text{b}}{140\ \text{nb}} = 210\text{-}290$

c) On the basis of these values let us assume that at high energy we have

$$\frac{\sigma(B\bar{B}X)}{\sigma(TX)} = 100$$

Hence, we estimate that for 400 (800) GeV/c πN interactions:

at 400 GeV/c ($\sqrt{s}$=27.4 GeV), $\sigma(B\bar{B}X) = 100\ \sigma(TX) = 100 \times 0.26\ \text{nb} = 26\ \text{nb}$

at 800 GeV/c ($\sqrt{s}$=38.8 GeV), $\sigma(B\bar{B}X) = 100\sigma(TX) = 100 \times 0.79\ \text{nb} = 79\ \text{nb}.$

We now consider some of the theoretical predictions for $B\bar{B}$ production cross sections. Figure 1 (upper part) shows the lowest order QCD diagrams for the heavy flavor creation of $b\bar{b}$ quarks in π^-p and $\bar{p}$p interactions [1,49]. Analogous diagrams hold for $c\bar{c}$ production. There are also two other diagrams (shown in the lower part of Figure 1) which could, in principle, contribute

to $c\bar{c}$ or $b\bar{b}$ production. Figure 1(e), corresponding to the fusion of light (u,d,s) $q\bar{q}$ pairs annihilating to ψ, is negligible because of the (Zweig's rule) coupling $g^2_{q\bar{q}\psi}/4\pi \approx 10^{-5}$. Figure 1(f) shows the fusion of heavy quarks to produce ψ. Here the coupling is not so small, $g^2_{c\bar{c}\psi}/4\pi \approx 0.5$, but the small heavy quark sea enters the cross section quadratically, so this diagram also gives a negligible contribution [1]. As a result, only the first four diagrams of Figure 1 contribute. Note [1], that since Figure 1(d) is not gauge invariant, diagrams 1(b and c) are also needed. Furthermore, the relative weight of the $q\bar{q}$ and gg contributions is fixed by the quark and gluon content of the mesons. Since

$$M^2 = sx_1x_2,$$

qualitatively we expect that the contributions from the gluon-gluon fusion diagrams Figure 1(b-d) should be suppressed and the valence $q\bar{q}$ annihilation mechanism should dominate at low energies. Since the gluon spectrum in hadrons is rather soft, the gluon fusion mechanism should become more important at high energies. For pN data, presumably the process will be due to gluon fusion. These ideas can be tested by comparison of ψ production by different beams and by measurements of the x_F distributions of ψ production. These comparisons with data show that [50]

i) $q\bar{q}$ annihilation alone cannot reproduce the trend of the data, but that the two processes combined give good agreement.

ii) for K^+ and p, which do not contain valence $\bar{u}$ or $\bar{d}$ antiquarks, gg fusion dominates at all energies, while

iii) for $\pi^\pm$, $\bar{p}$, K^- beams $q\bar{q}$ dominates at low energies (for $\sqrt{s} \leq 10$ GeV) and the gg process dominates at high energies.

From various theoretical calculations we find:

$$\sigma(pp \to BX) \sim 10\text{nb at } 400 \text{ GeV/c}$$
$$\sim 60\text{nb at } 800 \text{ GeV/c.}$$
$$\sigma(\pi^- p \to BX) \sim 15\text{nb at } 400 \text{ GeV/c}$$
$$\sigma(\bar{p}p \to BX) \sim 80 \text{ nb at } 800 \text{ GeV/c.}$$

In summary, both the phenomenological analyses and QCD calculations seem to agree on the approximate cross sections that one might expect to find:

$$\sigma(\pi N \to B\bar{B}X) \sim 25 \text{ nb at } 400 \text{ GeV/c}$$
$$\sim 80 \text{ nb at } 800 \text{ GeV/c, and}$$
$$\sigma(pN \to B\bar{B}X) \sim 10 \text{ nb at } 400 \text{ GeV/c}$$
$$\sim 60 \text{ nb at } 800 \text{ GeV/c.}$$

Experimental Results on B-Meson Production

At the current time only three experiments have reported limits on B-meson production:

a) WA 11 group: This experiment triggered on $\psi \to \mu^+\mu^-$ using 150 and 175 GeV/cπ^-N interactions at the CERN SPS. Originally [51] they presented evidence (based on 9000 ψ's) for a $\psi K^\circ\pi^\pm$ state with a mass of 5.3 GeV. The rough cross section estimate was $B\sigma \simeq 2$nb/nucleon. After doubling their sample (17,700 ψ's) in November, 1979 [52], the significance of the signal had decreased and $B\sigma \sim 1.7$ nb. Their latest data (based on 40,000 ψ's) correspond [3] to $\sigma_{B\bar{B}} \cdot B(B \to \psi K^\circ\pi^\pm) < 0.51$ nb and $\sigma_{B\bar{B}} \cdot B(B \to \psi K^\circ) < 0.08$ nb. Using $B(B \to \psi K^\circ\pi^\pm) \sim 1\%$, the most recent data thus suggest a total production cross section limit of $\sigma_{B\bar{B}} < 51$ nb.

b) Stanford-Cal Tech: From a study of a variety of multimuon final states in 400 GeV/c pFe interactions at Fermilab, this experiment [31] has set a limit of $\sigma_{B\bar{B}} < 50$ nb (with certain assumptions about decay modes yielding multimuons.)

c) Chicago-Illinois-Princeton: From a study [53] of 3μ final states in 225 GeV/c π^-N interactions at Fermilab, this experiment set a limit (with $B(\psi \to \mu^+\mu^-) = 0.07$ and a linear A dependence),

$$2\sigma_{B\bar{B}} \cdot B(B \to \psi X) \cdot B(B \to \mu X) < 81 \text{ pb/nucleon.}$$

With the estimate that $B(B \to \psi X) \sim 3\%$ and $B(B \to \mu X) = 12 \pm 4\%$, this yields $\sigma_{B\bar{B}} < 11$ nb.

In conclusion, we see that none of these experiments has seen a positive signal. However, their upper limits are not in disagreement with the cross sections expected at current energies. Hence, for calculations of event rates for this proposal we will use a cross section $\sigma_{B\bar{B}} = 50$ nb at 800 GeV/c.

Appendix IV

The High Resolution Streamer Chamber (HRSC)

The technique of the high resolution streamer chamber is a rapidly evolving one. The purpose of this appendix is to acquaint the reader with the current state of the art and with the future developments which are relevant to this proposal.

The E-630 Experience

The most advanced HRSC now in operation is the chamber currently (spring 1981) in use in E-630 at Fermilab. This chamber is a modified version of the first HRSC[1] which was developed at Yale and Fermilab and was used in E-490[2]. This chamber, and our experience with it, is the basis for our choice of HRSC parameters as listed in section IV of this proposal.

With the E-630 chamber we can operate, using the usual self luminous photography and high gain image tubes (optical gain = 10,000), at pressures of 40 atmospheres of Ne/He with pulsed electric fields of ~ 200 kV/cm and ~ 1 ns FWHM. Under these conditions the track width is dominated by diffusion of the "seed" electrons along the track and has a FWHM of ~ 200 μm in space. This diffusion limit would be improved by increasing the pressure but to do so would require proportionately greater electric field and greater strength in the pressure vessel. We have operated with good reliability for electric field values up to 400 kV/cm but basic limitations in the design and construction of the E-630 vessel have kept us from raising the pressure beyond 40 atmospheres.

We have instead added small admixtures of CO_2 to the gas. The large cross section for thermal (room temperature) electrons to scatter on CO_2 molecules causes the thermal diffusion of the electrons to be much depressed relative to the pure Ne/He (9/1) case. Figure 1 shows a track profile histogram taken with the Yale PEPR on a high energy muon track in the chamber with 3% CO_2 in 40 atmospheres (total) of Ne/He. The PEPR histogram is

taken in such a way that the track width and the effective PEPR spot diameter appear in sum (rather than in quadrature) in the profile. The effective spot width has been determined under the relevant PEPR operating conditions by measuring calibration lines and has been found to be 13.6 μm. The FWHM of the track is thus 50.7 μm on the film or 1.5x50.7 = 76 μm in space. This is very close to what one would expect "theoretically" using the previously measured values[3] for the diffusion coefficient of CO_2. Addition of the CO_2 has required a substantial increase in the electric field. The track of figure 1 was taken using a 355 kV/cm pulse. This represents a viable operating condition for E-630 and, except for slight increases of the CO_2 concentration , perhaps to 4.5% finally, will be the technology used for E-630.

We have also tried adding Xe to the gas instead of CO_2. Xe, like CO_2, has a large thermal cross section for electrons and should be effective in suppressing diffusion. Pure Xe admixtures of ~ 2% lead to spurious streamer growth and considerable optical background in the chamber. We understand the phenomenon in terms of the large photo-ionization cross section of Xe for the UV photons produced by the decay of excited neon atoms which are themselves a common species in the streamer. Under conditions we used, typical photo-ionization mean free paths were around 100 μm in the gas. This is a most troublesome value because the photons largely escape from the streamer but are virtually certain to launch a new streamer in the vicinity of the "old" streamer where the electric fields are space charge enhanced leading to rapid growth, etc.

Unfortunately, we did not have enough Xe to raise the concentration by a factor of 3 or 4 which should have made the photo-ionization mean free path short enough to remain inside the original streamer. We did verify this picture to some extent by adding 1% of CO_2 to the Ne/He/Xe mixture. The effect was a dramatic reduction of the background and indeed useable pictures were obtained with nearly "theoretical" values[3] of the diffusion limited track width. The CO_2 has a photo absorption cross

section only slightly lower than that of Xe, but CO_2 dissociates rather than photoionizes upon photon absorption. We abandoned further Xe studies for E-630 because of the greater economy of CO_2 relative to Xe, particularly for the rather large volume (23 ft^3) of the E-630 chamber. A very desirable feature of Xe as an additive is the fact that it does not raise the electric field required to operate the chamber.

One other area of E-630 experience is relevant to future chambers, namely our experience with the high voltage pulsing system. The E-630 system utilizes a parallel plate Blumlein pulse forming arrangement which for short pulses requires the simultaneous firing of 4 spark gaps if the theoretical maximum output voltage is to be obtained. We found that with our 1 Mw N_2 laser trigger we could fire two gaps but not three or four simultaneously. The pulse output with 2 gaps was not significantly better than that with one gap and we have decided to operate E-630 with only one gap switching the Blumlein. Under these conditions the output voltage is only 60% of the theoretical maximum (which is the voltage applied to the Blumlein just before the switch(es) fire).

Fortunately, we have found that fast switching times can be obtained with dry air as the spark gap gas. The operating voltage of air is very much greater than with the argon and nitrogen mixtures used previously. We are currently able to hold 310 kV on a 3.2 mm gap prior to spark gap firing. We have found that the switching times of almost all spark gap gases are about equal if the gap is operated so that breakdown occurs at the same applied voltage and the same gas pressure. We can thus confidently expect to switch ~ 500 kV either in the same length gap with the addition of "insulating" gases like SF_6 or simply, if necessary, by increasing the gap spacing somewhat.

Development Program for New HRSC Pulser

We believe that a single gap system, properly designed to match to one gap, can produce 500 kV on a 20Ω transmission line We have developed a conical, coaxial design which feeds a coaxial

to parallel plate transition to drive the (parallel plate) streamer chamber transmission line. We are currently carrying out detailed calculations and model studies on this design. We should follow this with a prototype pulser which will operate at nearly maximum voltage. We note that with pure Ne/He or with Ne/He/Xe a pulse of 500 kV on 20Ω is sufficient to operate a chamber of the dimensions listed in section IV. A pulse width of .5-1ns will be used.

Optics

The most important new development in streamer chamber technology is the use of holography to photograph the tracks. A Russian group[4] has already demonstrated holographic recording of an atmospheric pressure chamber and we note that optical inhomogeneity presented by the streamers scales as the cube of the pressure ratio. We thus expect our streamers to be as effective light scattering regions as is permitted by their size. In other words, streamer holography should be very similar to the holography of small bubble chambers.

The use of holography is, of course, essential if high resolution ($\lesssim$ 50μm) and large (~ 1 cm) sensitive depths are to be obtained simultaneously.

We propose to set up a small streamer chamber "test bed" at Yale to investigate and develop the techniques of holographic recording of high pressure streamers. Strictly speaking, the sensitivity of the holographic recording is such that the discharges should actually be in the avalanche rather than the streamer phase.

Finally, we note that in holographic recording the streamers appear much smaller[4] ($\sim\frac{1}{10}$) than they do in self luminous photography. This is to be understood, presumably, because they are recorded at a much earlier stage in their development. This means that, as is already the case in E-630, the track width is dominated almost entirely by diffusion of the electrons prior to the high voltage pulse.

Diffusion Suppression

There are two promising approaches to diffusion suppression. The approach we have used in E-630 and know the most about, involves the use of additions to the Ne/He gas. As an example we note that a 100 atmosphere chamber with 20% Xe would have a track FWHM of 36.4 μm in space if operated at room temperature. If the chamber were operated at 160°K (safely away from liquefaction) and if diffusion followed the classical $T^{-1/2}$ behavior we would expect 26 μm tracks.

The second approach is to investigate more carefully the effects of lower temperatures. A study of the literature of the drift and diffusion of electrons in cold gases has revealed some surprising results. In short, it appears that diffusion (and electron mobility at low electric fields) is drastically reduced at low temperatures relative to the classical expectation.[5] The theoretical explanation is that when the (thermal) electron DeBroglie wavelength becomes comparable to the (classical) scattering mean free path the simple, classical, picture breaks down and the electron interacts with many gas atoms at once and has drastically reduced mobility. So far, experiments are only available for pure Helium but one would expect very similar results for Ne or Ne/He mixtures.

Clearly, we wish to use our proposed streamer chamber test bed to study both approaches to the diffusion suppression. We note that if the low temperature effect works the final track width may be just a few microns. For the purposes of this proposal, we have used a 20-30 μm estimate which is a reasonable expectation for the additive approach.

Budgets and Schedules

Our basic approach to the development of the new HRSC is to first carry out a research and prototype program with our proposed streamer chamber test bed at Yale and then, on the basis of that experience, design and construct the chamber for the HQS. We estimate a budget for the development program as follows.

1. General, fast pulse, high voltage instrumentation		$30,000
2. Materials, supplies and labor for development of new pulsing system		35,000
3. Set up of Streamer Chamber Test Bed at Yale		
a. Marx Generator	30,000	
b. Materials and labor for test chamber	30,000	
c. Cryogenic equipment for low temperature studies	15,000	
d. Excimer laser for pumping holographic dye laser	35,000	
e. Holographic quality dye laser	20,000	
Sub Total		130,000
4. Component prototypes for HQS chamber		20,000
5. Contingency		25,000
Total		$240,000

We note that the test chamber would use our present, inefficient, parallel plate Blumlein system because that is more than adequate for a small chamber. Thus the additive, holography, and low temperature studies would be independent of the new pulser development and would proceed in parallel. They would (time) share the same Marx generator which could readily be moved from one set up to the other.

We would expect to have sufficient results after about one year of the test bed program to begin design and construction of the HQS chamber. We would undoubtedly continue working with the test bed throughout the entire period of constructing the HQS chamber. We believe that it is very reasonable to have the HQS chamber completed for the initial phase in early 1983.

References Appendix IV

1. "The High Resolution Streamer Chamber," J. Sandweiss, Physics Today, October 1978 and "Design and Performance of a High Resolution Streamer Chamber," R. Majka, et. al, to be published in Review of Scientific Instruments.

2. J. Sandweiss, et. al., Physical Review Letters 44, 1104 (1980).

3. "The Diffusion and Drift of Electrons in Gases," L.G.H. Huxley and R.W. Crompton, John Wiley and Sons, New York (1974).

4. V.S. Kozlov, et. al., Nuclear Instruments and Methods 140, (1977).

5. "Electron Localization in Dense Helium Gas: New Experimental Results," K.W. Schwartz, Physical Review B 21, 5125 (1980).

Figure 1 (Appendix IV)

PEPR profile histogram for a high energy muon track. The picture was taken with 40 atmospheres of Ne/He (9/1) with 3% CO_2.

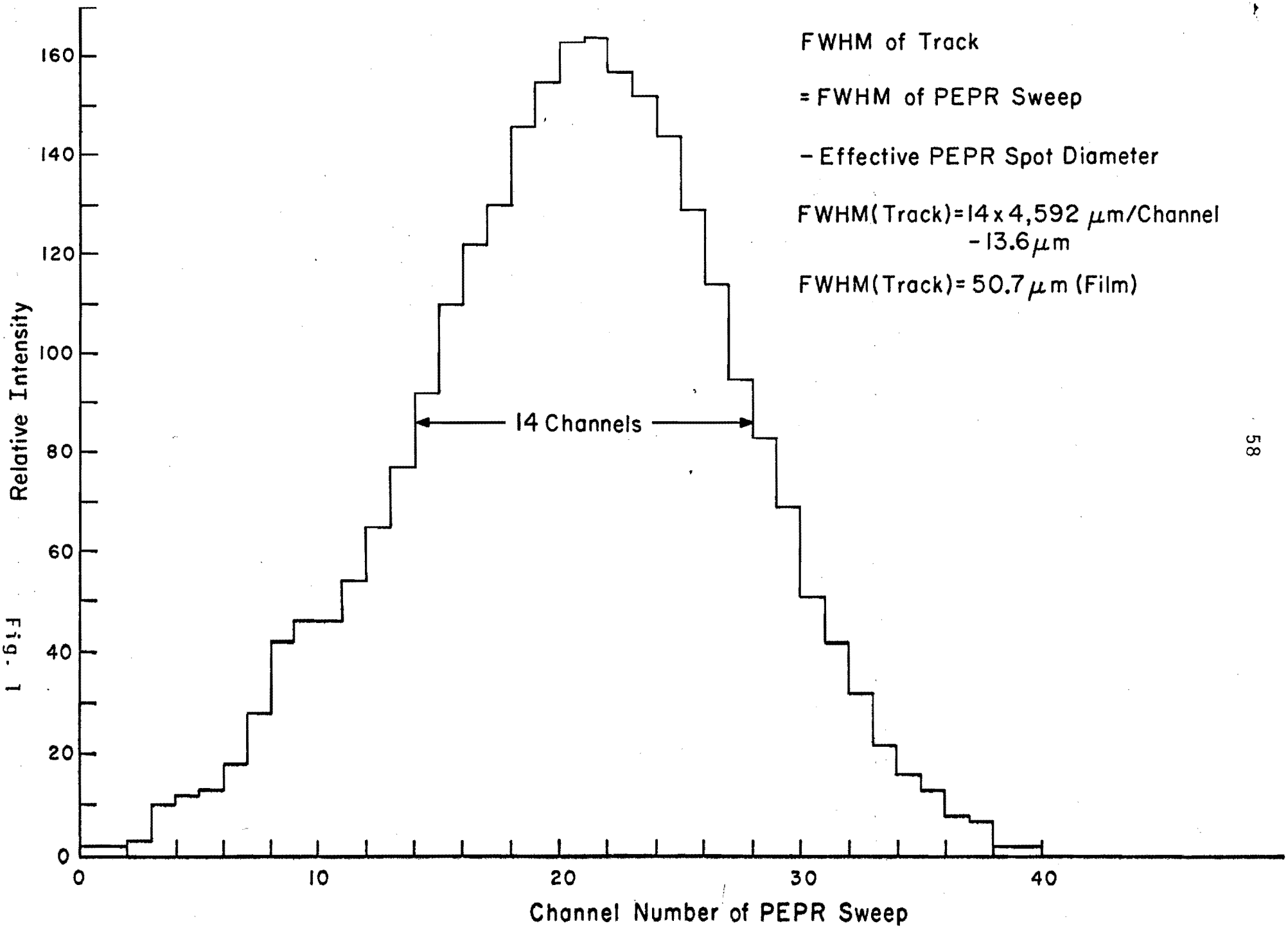
FWHM of Track
= FWHM of PEPR Sweep
- Effective PEPR Spot Diameter
FWHM(Track)=14 x 4,592 μm/Channel
-13.6μm
FWHM(Track)= 50.7μm (Film)
14 Channels
Relative Intensity
Channel Number of PEPR Sweep
0
20
40
60
80
100
120
140
160
0
10
20
30
40

Fig. 1